2020

Reverberation multiphoton microscopy for volumetric imaging in scattering media

BOSTON UNIVERSITY

COLLEGE OF ENGINEERING

Dissertation

REVERBERATION MULTIPHOTON MICROSCOPY FOR VOLUMETRIC IMAGING IN SCATTERING MEDIA

by

DEVIN R. BEAULIEU

B.S., Rensselaer Polytechnic Institute, 2011
M.S., Boston University, 2016

Submitted in partial fulfillment of the

requirements for the degree of

Doctor of Philosophy

2020

Approved by

First Reader _____

Thomas G. Bifano, Ph.D.
Professor of Mechanical Engineering
Professor of Materials Science and Engineering
Professor of Biomedical Engineering

Second Reader _____

Jerome C. Mertz, Ph.D.
Professor of Biomedical Engineering
Professor of Electrical and Computer Engineering
Professor of Physics

Third Reader _____

Lei Tian, Ph.D.
Assistant Professor of Electrical Engineering

Fourth Reader _____

Roger Dufour, Ph.D.
Associate Group Leader
MIT Lincoln Laboratory

ACKNOWLEDGEMENTS

First and foremost, I would like to thank Dr. Thomas Bifano, who has been an excellent advisor and has supported me through both my masters and now my doctorate programs. I would also like to thank Dr. Jerome Mertz, who has taught me everything I know about microscopy and has effectively been a second advisor in my research. Both have made my research into an enjoyable and rewarding experience, and I have learned a great deal from both.

Next, I would like to thank my wife Courtney Sullivan, who has been a huge support in taking on the stress of graduate school.

I would also like thank our collaborators, Ian Davis, Kıvılcım Kılıç, Christos Michas, Clemens Riegler, and Shoshana Das. All of whom gave their own time to provide me with awesome samples to look at as I developed and tested the reverberation technique. Thank you as well to Helen Fawcett, for the extra effort in getting paperwork sorted so for our tissue experiments as well as making sure that research could continue during our lab renovations.

Finally, I would like to thank the great number of people at Lincoln Laboratory who have helped and supported me in getting back to school to continue my education. This includes Dr. Thierry Copie, Dr. Roger Dufour, Dr. Aryeh Feder, and everyone else who devoted their time and energy to help me succeed at both Lincoln and BU. This dissertation would not have been possible without the support I have received from the Laboratory and the Lincoln Scholars Program.

REVERBERATION MULTIPHOTON MICROSCOPY

FOR VOLUMETRIC IMAGING IN SCATTERING MEDIA

DEVIN R. BEAULIEU

Boston University College of Engineering, 2020

Major Professor: Thomas Bifano, Professor of Mechanical Engineering, Professor of Materials Science and Engineering, Professor of Biomedical Engineering

ABSTRACT

Multiphoton microscopy has become an extremely valuable tool for peering deeply into thick, scattering media such as biological tissue. However, the traditional multiphoton beam-scanning approach is held back because only one thin plane is observed at a time. The reverberation loop elegantly overcomes this limitation by generating an infinite series of foci at depths spanning the sample, all sampled individually but near-simultaneously. With the inclusion of some additional interleave steps, it is possible to quickly scan a sample at video rates – allowing volumetric imaging at or near the rate one would traditionally image planes. In neural imaging, this enables a reverberation multiphoton microscope to simultaneously monitor relationships in neuronal activity not only horizontally across samples, but vertically across many layers of the brain. In imaging of engineered cardiac tissues, this enables high resolution observation of three-dimensional structures in a live sample, even as it actively beats and moves.

TABLE OF CONTENTS

LIST OF TABLES

LIST OF FIGURES

LIST OF ABBREVIATIONS

2PM	Two Photon Microscopy
3PM	Three Photon Microscopy
BS	Beamsplitter
DOF	Depth of Focus
FITC	Fluorescein Isothiocyanate
FOV	Field of View
FPGA	Field-Programable Gate Array
FWHM	Full Width at Half Maximum
GCaMP	GFP Calmodulin Protein
GDD	Group Delay Dispersion
GECI	Genetically Encoded Calcium Indicator
GFP	Green Fluorescent Protein
GVD	Group Velocity Dispersion
HPD	Hybrid Photodetector
MPM	Multiphoton Microscopy
NA	Numerical Aperture
PMT	Photomultiplier Tube
PSF	Point Spread Function

INTRODUCTION

Multiphoton microscopy (MPM) has gained enormous popularity over the years for its capacity to provide high resolution images from deep within scattering samples (Helmchen and Denk 2005). However, MPM is generally based on single-point laser-focus scanning, which is intrinsically slow. While imaging speeds as fast as video rate have become routine for 2D planar imaging, such speeds have so far been unattainable for 3D volumetric imaging without severely compromising microscope performance (Ji, Freeman, and Smith 2016). A new technique presented here, called reverberation MPM, allows 3D volumetric (multiplane) imaging at the same speed as 2D planar (single plane) imaging, with minimal compromise in performance. Specifically, multiple planes are acquired by near-instantaneous axial scanning while maintaining 3D micron-scale resolution. The technique is well adapted for large-scale imaging in scattering media with low repetition-rate lasers, and can be implemented with conventional MPM as a simple add-on.

BACKGROUND

Imaging inside scattering media is a challenging problem, but one which is unfortunately faced in many samples of interest. In particular, biological tissues such as brain, heart, and others scatter light as it passes through, making it difficult to image what occurs under the surface. MPM is one technique which can be used to increase imaging depth over that of standard microscopy.

Traditional widefield fluorescence microscopy illuminates the entire

sample with light. The color of the light is selected to match the absorption spectrum of whatever fluorescent fluorophore is in use. The light re-emitted by excited fluorophores is collected, and them imaged onto a camera. This approach works well in a clear sample but begins to break down as scattering is introduced. As the emitted light exits the sample, much of it is scattered, making the image appear blurred; progressively more blur occurs as imaging depth increases. (As the entire sample is illuminated, scattering of the illumination light is largely irrelevant in this case.)

MPM combines optical scanning with nonlinear effects to mitigate the effects of scatter. Firstly, only a single point in the sample is illuminated at any given time with sufficient intensity to produce two photon excited fluorescence. It is assumed that all light emitting from the sample originates from that single illuminated spot – regardless of where it appears to come from. Intensity of the emitted light is then measured as the point scans the sample to generate an image. By measuring light exiting the sample in bulk (rather than imaging onto a camera) the effect of scattering on the emitted light is minimal. However, scattering of the illumination beam is now a concern, as it will increase the size of the illuminated spot or scatter to elsewhere in the sample. This is why a multi-photon nonlinear effect is used. In the two-photon case, rather than illuminating with a wavelength in the absorption band, light with twice this wavelength (i.e. half the energy) is used. This light can still be absorbed, but will require two photons per interaction instead of one. Critically, nonlinear optics indicates that

the intensity of emitted light will depend on the square of the illumination intensity, rather than being directly proportional. Illumination light which has scattered elsewhere in the sample will generate comparatively little fluorescence, so the emitted signal will be dominated by the un-scattered (ballistic) light at the focus.

The standard method for obtaining volumetric images with MPM is to perform x-y scanning with galvanometric mirrors, and then z-scanning by adjusting the microscope objective; this is slow and cumbersome. Faster volumetric imaging can be obtained by purposefully decreasing image resolution (Prevedel et al. 2016), or by using faster z-scanning mechanisms, such as electrically tunable lenses (Grewe et al. 2011), deformable mirrors (Shain et al. 2017), voice-coils (Sofroniew et al. 2016), or tunable acoustic gradient (TAG) lenses (Olivier et al. 2009). For example, although TAG can provide axial scan rates at tens of kilohertz, it comes at the cost of limited depth range (Kong et al. 2015).

Alternatively, simultaneous multifocus (W. Yang et al. 2015), extended focus (Theriault, De Koninck, and McCarthy 2013; Lu et al. 2017) or stereoscopic (Y. Yang et al. 2016; Song et al. 2017) illumination can be achieved by wavefront engineering, providing 2D images of volumetric samples obtained from single transverse scans. While fast, these solutions sacrifice axial resolution by yielding only 2D projections. Axial localization and segmentation can be calculated post acquisition, but with the requirement of computational models and/or a priori

knowledge about the sample structure. Consequently, such solutions involving simultaneous multiplexed illumination are best suited for sparse samples.

The use of high-speed detection electronics has opened new approaches for near-simultaneous multiplexing, taking advantage of the ability to individually measure fluorescence signals a few nanoseconds apart. This has been implemented in previous work by separating the illumination beam into a few (usually two) beamlets of different pathlengths (Amir et al. 2007; Hu et al. 2018; Cheng et al. 2011; Chen et al. 2016; Stirman et al. 2016). In this manner, the signals produced by each beamlet can be separated in time using fast detection electronics. By focusing each beamlet to a different depth within the sample, a near simultaneous focal stack can be obtained from a single transverse scan. However, such multiplexing becomes technically cumbersome with increasing number of beamlets, and leads to laser power loss when the number of beamlets is greater than two (unless the focal planes are staggered in the transverse direction (Cheng et al. 2011)). A similar multiplexing approach has been implemented in the detection optics of a camera-based imaging system (Heshmat et al. 2018).

REVERBERATION MICROSCOPY

Reverberation microscopy is a simplified alternative to the above temporal multiplexing solutions. This more general approach provides an infinite series of beam foci, performing a near-instantaneous axial scan, while delivering the full illumination power to the sample.

For each laser pulse, the reverberation loop creates an infinite series of beam foci separated in space and time. Six are shown in the schematic below (Figure 1), with the subsequent plane terminated by the surface of the sample. The spatial separation between each focus in the sample can be controlled as desired without affecting alignment by adjusting the pathlength of the loop (the left pair of mirrors and lenses in the loop are mounted on a linear translation stage to facilitate this adjustment).

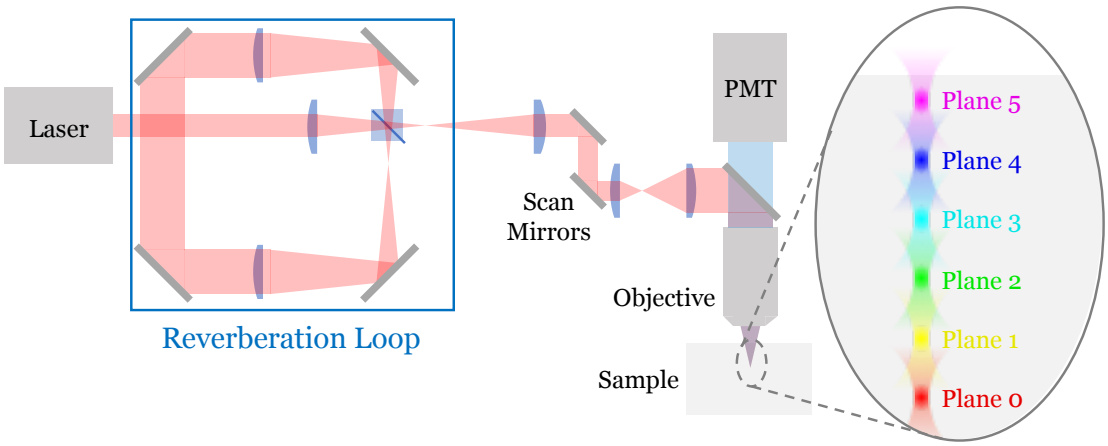

Figure 1. Reverberation MPM schematic.

The optical configuration is typical of MPM setups except for the addition of a reverberation loop upstream from the beam steering mirrors. Here a 50:50 non-polarizing beamsplitter splits the illumination beam, with half the light proceeding to the sample normally, and the other half entering the loop. The 1× relay in the loop is intentionally mis-adjusted (spaced too far apart) so that a small amount of focus is added to the beam. Upon returning to the beamsplitter half of the light exits the loop and proceeds to the sample, but now with a modified focus and time delay (due to the time spent in the loop). The light

remaining in the loop continuously repeats the process, accumulating slightly more focus and delay upon each pass.

As a result of the reverberation loop, each laser pulse produces a series of beam foci of decreasing depth within the sample that arrive sequentially in time. In MPM, only the ballistic (i.e. un-scattered) portion of this power contributes to fluorescence generation (Helmchen and Denk 2005). The relative fluorescence power produced at each focal spot is thus given by equation 1, where m is the nonlinear order (2 for two-photon microscopy), l_s is the scattering mean-free-path at the illumination wavelength, and fluorescence labeling density is assumed to be roughly homogenous.

$$F_n = F_0 \exp\left(mn\left(\frac{\Delta z}{l_s} - \ln(2)\right)\right) \quad (1)$$

In other words, even though the incident power associated with each focal spot decreases geometrically with decreasing depth (increasing n), the resulting fluorescence may or may not decrease depending on our choice of plane spacing (Δz). For example, if the inter-plane spacing is chosen such that $\Delta z = l_s \ln(2)$, the decrease in scattering at shallower depths exactly compensates for the decrease in incident power with increasing n, and the fluorescence produced from each focal spot remains roughly constant at all depths. On the other hand, if a finer inter-plane spacing is desired (i.e. $\Delta z < l_s \ln(2)$), the fluorescence becomes successively dimmer with shallower depths, which can be corrected in post

processing provided the detector supplies adequate dynamic range.

Figure 2 illustrates the timing of the illumination and fluorescence pulses, with a different color indicating each focal depth. Here, Δz is chosen so that the reduction in illumination power between planes is exactly offset by the reduction in scattering from shallower foci. This example shows the timing of a 2 m long reverberation loop, giving a 6.7 ns delay between focal depths – sufficient spacing to measure each individually with a high-speed amplifier and digitizer. Also note that the 20 MHz laser pulse rate leaves room for seven reverberation pulses (planes) between each laser pulse.

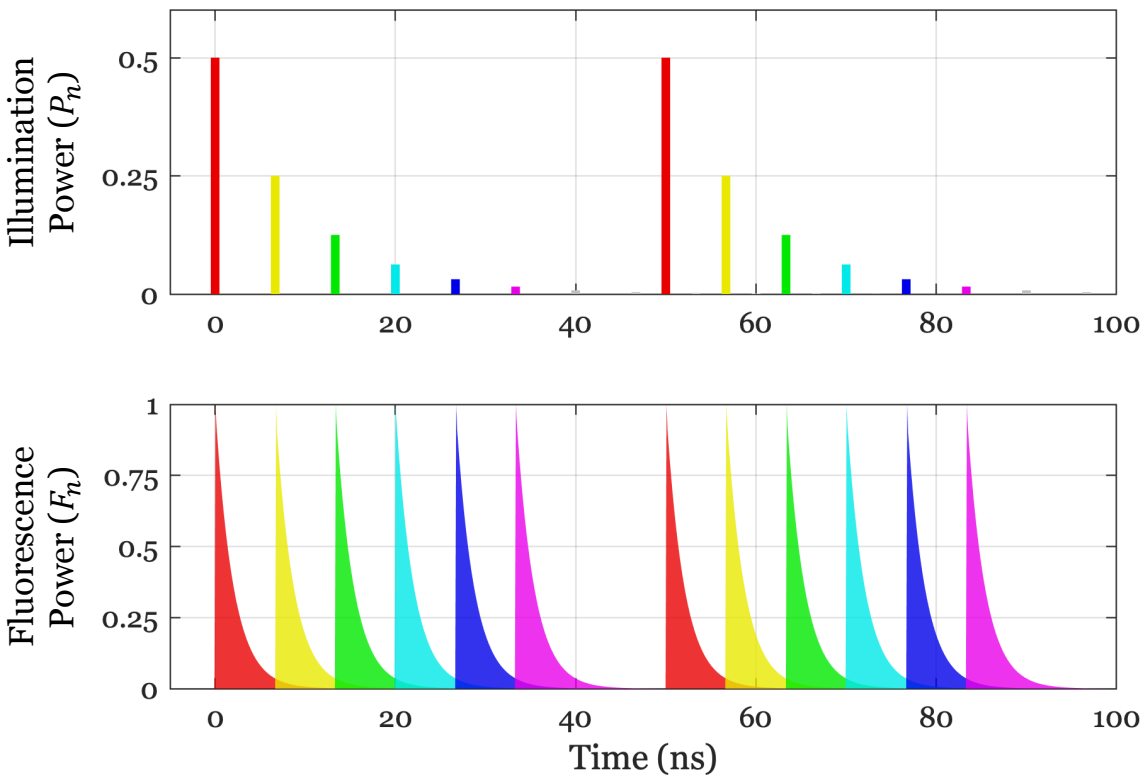

Figure 2. Timing and power of illumination pulses and corresponding fluorescence signals.

In theory, the pulse reverberation subsists indefinitely (with decreasing power), producing an arbitrary number of focal depths. In practice, the sequence of focal depths is terminated at n when the $(n+1)$-th focal spot exits the sample, thus terminating the sequence of fluorescence and preventing it from overlapping with signal from the next laser pulse (alternatively, if $\Delta z < l_s \ln(2)$, the fluorescence can fade away before such overlap occurs).

It is also important to bear in mind that the fluorescence lifetime of fluorescent indicators is typically a few nanoseconds (Berezin and Achilefu 2010). To properly distinguish the signal from successive focal spots, the time delay between these should be longer than the fluorescence lifetime. This effect can be observed in Figure 2, where the 4 ns lifetime leads to a small amount of crosstalk between the reverberation pulses which are 4.7 ns apart. Note that most of this crosstalk can be removed in post-processing, by subtracting a proportion of the previous plane from each plane.

The dual constraints of maximizing number of planes between laser pulses while minimizing inter-plane fluorescence crosstalk motivate the use of lasers with slower repetition rates and correspondingly higher pulse powers. As it happens, such lasers are advantageous for deep imaging (Theer, Hasan, and Denk 2003; Beaurepaire, Oheim, and Mertz 2001), and even indispensable for three-photon imaging (Horton et al. 2013).

REVERBERATION MICROSCOPY THEORY

Beamsplitter Selection

There is some subtlety to the choice of a 50:50 beamsplitter for the reverberation loop which warrants further discussion. The power decay rate of the reverberation planes is determined by the split ratio of the loop beamsplitter. This decay appears as the $\ln(2)$ term in equation 1, indicating a factor of two drop with each pass (i.e. a 50:50 beamsplitter). It may initially appear possible to use a slower decay rate to achieve tighter spacing – since $\Delta z \sim l_s \ln(2)$ – however, it is not this simple in practice.

With a 50:50 beamsplitter the power sequence is 0.500, 0.250, 0.125, 0.063, etc. This is a uniform geometric decay law that is well matched to the exponential fall-off of the excitation power required at the decreasing depths given by our Z-plane spacing. Use of other ratios is problematic as the first pulse does not follow the geometric decay.

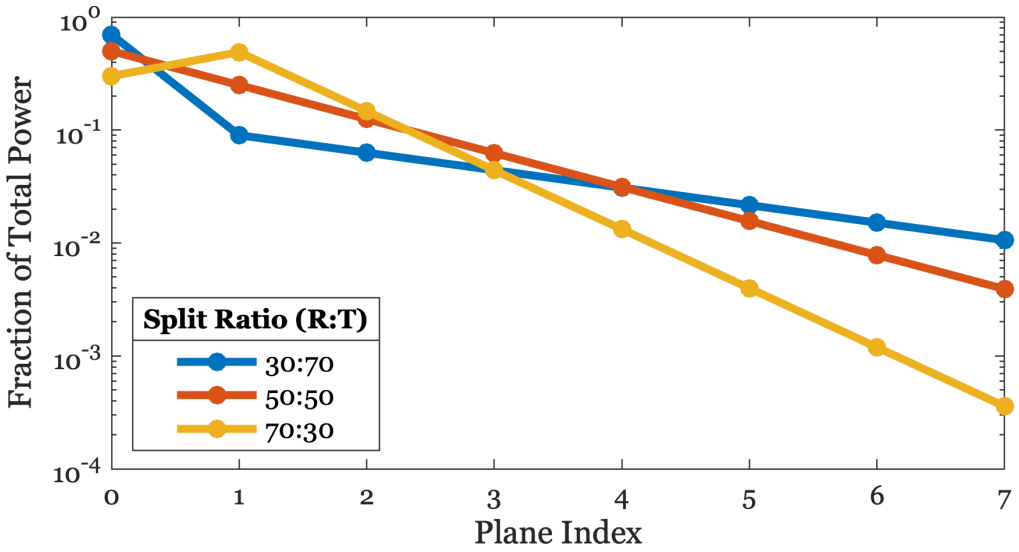

Figure 3. Reverberation power decay for several beamsplitter options.

For example, with a 10:90 beamsplitter, the power sequence becomes 0.900, 0.010, 0.009, 0.008, etc. This has a slower decay after the first pulse (leading to tighter plane spacing), but the very strong first pulse will cause tissue damage and/or overload the PMT. Alternatively, with a 90:10 beamsplitter, the power sequence is 0.100, 0.810, 0.081, 0.008, etc. Here the first pulse is too weak to be used. Furthermore, the decay is very rapid, leading to imaging planes which are undesirably far apart. Neither of these scenarios are desirable, hence the intentional use of a 50:50 beamsplitter.

Resolution and Plane Thickness

While thicker imaging planes may be desirable to increase the z-depth sampled by each plane, this comes with the unfortunate side effect of decreased xy-resolution. This conclusion can be drawn directly from the dependency between illumination beam width (W_0) and depth of focus ($2z_0$) for Gaussian

beams (Saleh 2007, 80):

$$2z_0 = \frac{2\pi W_0^2 n}{\lambda} \tag{2}$$

A slightly more thorough derivation is necessary to explore this trade-off and directly relate the imaging resolution to a relevant microscope system parameter (i.e. numerical aperture). This begins with the description of a generic Gaussian beam (Saleh 2007, 77–80):

$$\begin{gathered} I(\rho, z) = I_0 \left(\frac{W_0}{W(z)}\right)^2 \exp\left(-\frac{2\rho^2}{W(z)^2}\right) \\ W(z) = W_0 \sqrt{1 + \left(\frac{z}{z_0}\right)^2} \\ \theta_0 = \frac{\lambda}{\pi n W_0} \end{gathered} \tag{3}$$

It is useful to redefine the gaussian beam based on the numerical aperture (NA) of the optical system:

$$\begin{gathered} NA = n \sin(\theta) \approx n\theta \\ W_0 = \frac{\lambda}{\pi n \theta_0} \approx \frac{\lambda}{\pi NA} \\ z_0 \approx \frac{\lambda n}{\pi NA^2} \end{gathered} \tag{4}$$

Multi-photon fluorescence has a finer resolution than that of the illumination beam itself, as the emission is proportional to the square of the intensity, so this must be taken into account. The two-photon fluorescence (F) from a Gaussian beam illumination is given as follows:

$$F(\rho,z) \propto I(\rho,z)^2 = I_0^2 \left(\frac{W_0}{W(z)}\right)^4 \exp\left(-\frac{4\rho^2}{W(z)^2}\right) \tag{5}$$

The two-photon fluorescence depth of focus (DOF) can then be derived, defined here as the on-axis full width at half maximum (FWHM):

$$\begin{gathered} \frac{1}{2}F(0,0) = F\left(0,\frac{DOF}{2}\right) \\ DOF \approx 0.41\frac{\lambda n}{NA^2} \end{gathered} \tag{6}$$

Likewise, for the two-photon fluorescence xy spot size ($\varnothing_{spot}$), defined here as the FWHM at the focus:

$$\begin{gathered} \frac{1}{2}F(0,0) = F\left(\frac{\varnothing_{spot}}{2},0\right) \\ \varnothing_{spot} \approx 0.27\frac{\lambda}{NA} \end{gathered} \tag{7}$$

These results can be combined for the plot shown in Figure 4, which reveals the explicit tradeoff between spot size and plane thickness as determined by the NA of the system. This plot assumes a wavelength of 1 μm and index of refraction of 1.3.

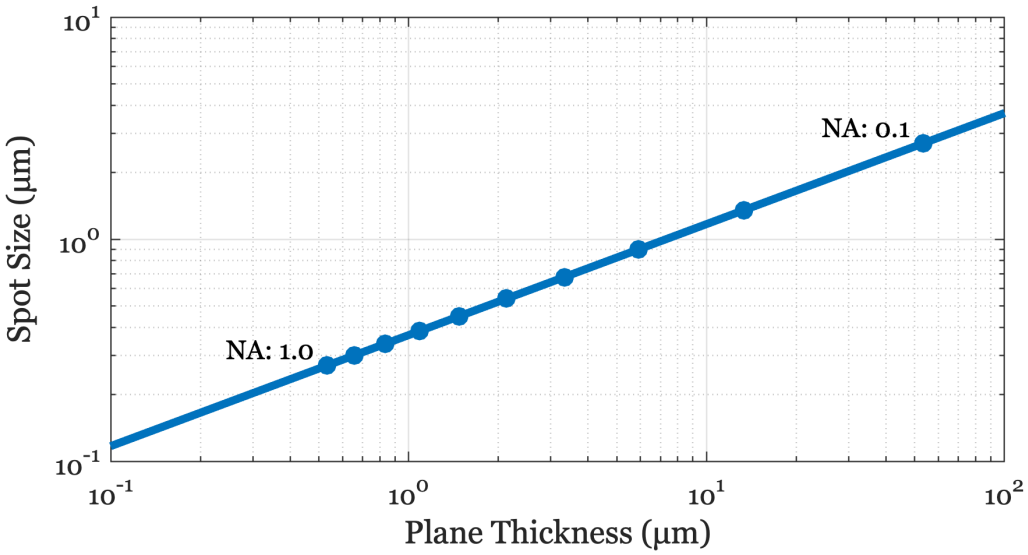

Figure 4. Tradeoff between spot size and plane thickness for varying numerical aperture.

Figure 4 reveals why it is impractical to achieve continuous sampling on a reverberation setup simply by using thick planes. With scatter lengths (and therefore plane spacing) commonly on the order of 100 μm, the spot size grows to 4 μm, which is likely undesirably large for many applications. However, with a combination of interleaved pulses and a two-depth stage scan, the needed thickness is quartered to 25 μm, giving a somewhat more reasonable 1.8 μm spot size.

REVERBERATION SYSTEM DESIGN

The design of the reverberation loop requires special attention to obtain good beam quality throughout all imaging planes. With eight or more passes through the loop, and the corresponding large shifts in focal depth, unintended aberrations can rapidly stack up. Additionally, as will be seen shortly, the focal shifts can lead to foci occurring near (or within) optical elements, with potentially

undesirable consequences. The following subsections will walk through a complete analysis of two design options, one where the loop is introduced at the pupil plane and the other where it is introduced at the image plane. While both approaches are viable, there are tradeoffs between the two designs.

These exemplar designs will assume the same system parameters and loop requirements (i.e., they are functionally equivalent), as outlined in Table 1. These specifications are directly applicable to those of the prototype microscopes described in the results section, although in practice the plane spacing and count varies from sample to sample.

Objective Magnification / Focal Length ($f_{objective}$)	16× / 12.5 mm
Scan/Tube Lens Magnification ($M_{scan-tube}$)	2×
Input Aperture Diameter ($\varnothing_{aperture}$)	5 mm
Number of Planes (n)	8
Plane Spacing (Δz)	100 μm
Total Imaging Volume Depth (ΔZ)	700 μm (±350 μm)
Loop Length / Period	2.0 m / 6.7 ns

Table 1. System parameters and requirements for notional reverberation microscope.

Note that there is an implicit relationship between the number of planes, plane spacing, and total imaging volume depth:

$$\Delta Z = (n-1)\Delta z \tag{8}$$

Basic Design & Layout

The basic layout of a reverberation loop is fairly simple, consisting of a rectangular optical loop, a pair of loop lenses, and a pair of relay lenses. If the beam splitter is located at the image plane the relay lenses are placed outside the

loop (Figure 5), while if the beam splitter is at the pupil plane they are placed inside the loop (Figure 6).[1]

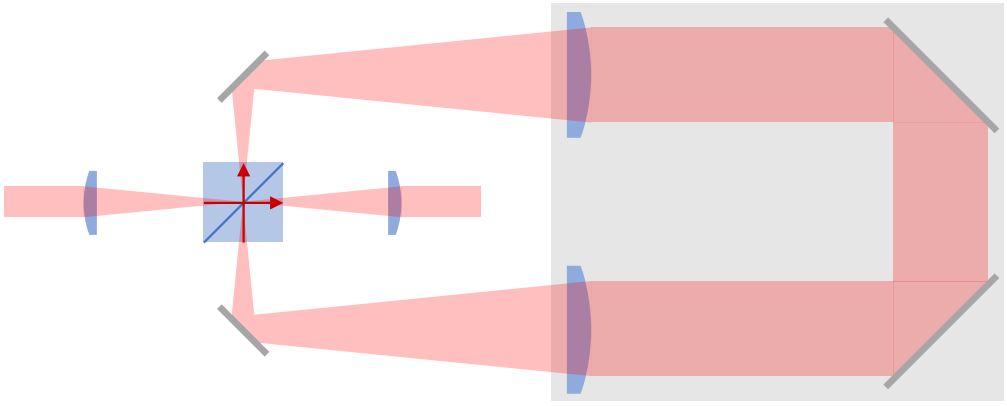

Figure 5. Diagram of generic reverberation loop, with beam splitter in image plane.

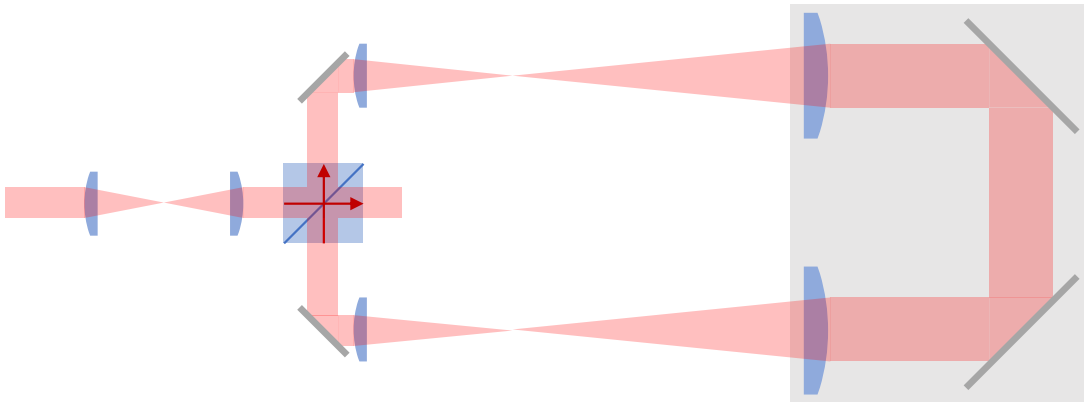

Figure 6. Diagram of generic reverberation loop, with beam splitter in pupil plane.

[1] During the course of our research, we successfully built reverberation microscopes based on both of these concepts. Our first implementation had the BS in the pupil plane. However, we could only achieve a limited number of reverberation planes – aberrations started to accumulate quickly, as we had not yet thought to center the reverberation foci around the loop's ideal focus (see dashed line in Figure 12). We initially solved the aberration problem by moving the BS adjacent to the image plane, but having the BS so near the foci is not ideal and several splitters were accidentally blown up due to incorrect alignment. While the pupil BS design experiences somewhat more aberration (see solid lines in Figure 12), this may be an acceptable compromise to get the beamsplitter away from all foci while still achieving as many reverberation planes as needed.

In these diagrams a collimated laser beam enters the loop from the left, while the output pupil is placed in conjugate (or relayed) to the steering galvanometers. In both cases, the loop lenses and far mirrors are placed on a movable stage to control the plane spacing; additionally, a lens prior to the loop translates to control the depth of the initial focus relative to the normal focus point. Note that in practice the full-power beam is never focused directly onto the beam splitter as depicted in Figure 5, as the initial focus would be placed somewhere past the optic.

Timing and Image Readout

Timing and synchronization play key roles in reading out each reverberation plane individually. This involves syncing of the laser and digitizer, with additional benefits from ensuring the reverberation pulses are synchronized as well.

The basic timing/sampling configuration is similar to the acquisition gating approach which can be performed in general MPM setups to improve signal to noise. With low repetition rate lasers, there is a significant amount of dead time between each laser pulse with no signal (on the order of 100 ns), while the fluorescence comes in a short burst lasting only a few nanoseconds. Acquisition gating is used to only record during the time of fluorescence, effectively eliminating all noise from periods without signal. In reverberation microscopy, the approach is the same just with multiple, sequential bursts of fluorescence (corresponding to each plane) for each laser trigger. Each

fluorescent burst is recorded separately as a different channel to preserve depth information.

A clock generator is used to upconvert the laser clock to a reasonable sampling rate to ensure at least one sample per reverberation plane.[2] The synchronization of these clocks makes sure that the fluorescent signals do not drift relative to the sampling times. (While triggering off the laser pulses keeps everything approximately in sync, without syncing the sample clock as well the relative phasing can drift and affect how the signal is discretized into sampling bins.)

It is also beneficial to have the sampling rate be a multiple reverberation pulse rate (the rate pulses come out of the reverberation loop, as determined by the loop length). This means the number of samples per plane will be a whole number and, more importantly, each plane will be sampled with consistent phasing relative to sampling bins. While not strictly necessary, this step is particularly helpful for reducing the effect of discretization artefacts when doing crosstalk removal to separate overlapping plane responses.

Lens Selection & Ray Tracing

There are two lens focal lengths for specifying the reverberation loop. The first is the relay lens (f_{relay}), which determines the magnification (M_{loop}) from

[2] Specifically, we used an Analog Devices AD9516 to multiply the laser clock to 1200 MHz. This happens to be a convenient multiple for all of the lasers we used (80 MHz Chameleon, 10 MHz Fidelity, and 1 MHz Opera), while conveniently also being a multiple of the repetition rate of 1 and 2 m long optical loops (300 MHz and 150 MHz).

the objective's image plane to the loop's focus. The reverberation loop is configured to slightly shift the focal point within the loop on each pass (by Δz_{loop}) causing a corresponding shift (Δz) in the image plane. However, since there is a magnification, the shift is amplified:

$$M_{loop} = M_{scan-tube} \frac{f_{relay}}{f_{objective}} \tag{9}$$

$$\Delta z_{loop} = M_{loop}^2 \Delta z \tag{10}$$

The loop magnification is critical, as it affects both the total amount the focus will need to shift within the loop (ΔZ_{loop}) to achieve the desired shift in the image – Equation 11, and also how large the beam diameter ($\varnothing_{loop}$) will become – Equation 12. Too high a magnification and the focus can shift into and through the relay lens (when $\Delta Z_{loop}/2 \geq f_{relay}$) likely leading to aberrations, while too low and the beam can become unmanageably large.

$$\Delta Z_{loop} = M_{loop}^2 \Delta Z = \left(M_{scan-tube} \frac{f_{relay}}{f_{objective}} \right)^2 \Delta Z \tag{11}$$

$$\varnothing_{loop} = \varnothing_{aperture} \frac{f_{loop} + \Delta Z_{loop}/2}{f_{relay}} \tag{12}$$

The other focal length, that of the loop lenses (f_{loop}), primarily sets the length of the loop; this length is more flexible, but longer loops do require larger optics (see Equation 12).

Both of these constraints are plotted in Figure 7, with some reasonable

restrictions shaded in red.

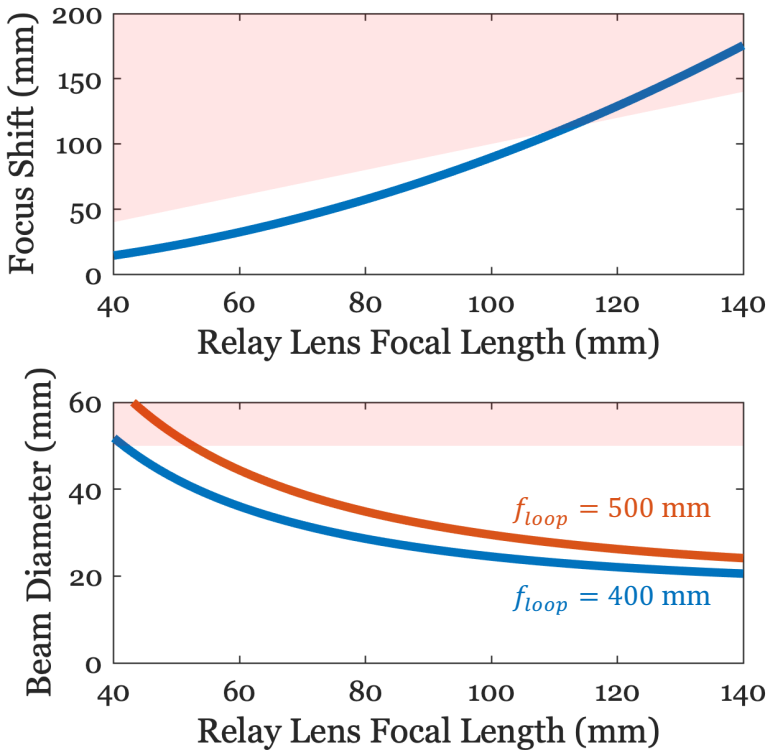

Figure 7. Bounding limits of relay lens focal length for setup specified in Table 1.

Selecting a relay lens focal length effectively sets the remainder of the properties of the loop. The properties for a 100 mm relay lens (given the requirements from Table 1) are summarized in Table 2. Note that in this case f_{loop} differs depending on the beam splitter (BS) location so that both setups will have the same total loop length.

Relay Lens Focal Length (f_{relay})	100 mm
Loop Lens Focal Length (f_{loop})	500 mm (BS in Image Plane) 400 mm (BS in Pupil Pupil)
Loop Image Demagnification (M_{loop})	16×
Loop Focal Spacing (Δz_{loop})	25.6 mm
Loop Total Focal Depth (ΔZ_{loop})	179 mm

Table 2. Selected and derived loop parameters for notional reverberation microscope.

With all the relevant parameters defined, it is possible to trace out the path of light through the loop, as seen in Figure 8 and Figure 9. The vertical blue lines indicate lens locations, while the colored set of lines shows the path of the beam for each reverberation plane from the 0th (red, which does not enter the loop) through 7th (magenta).

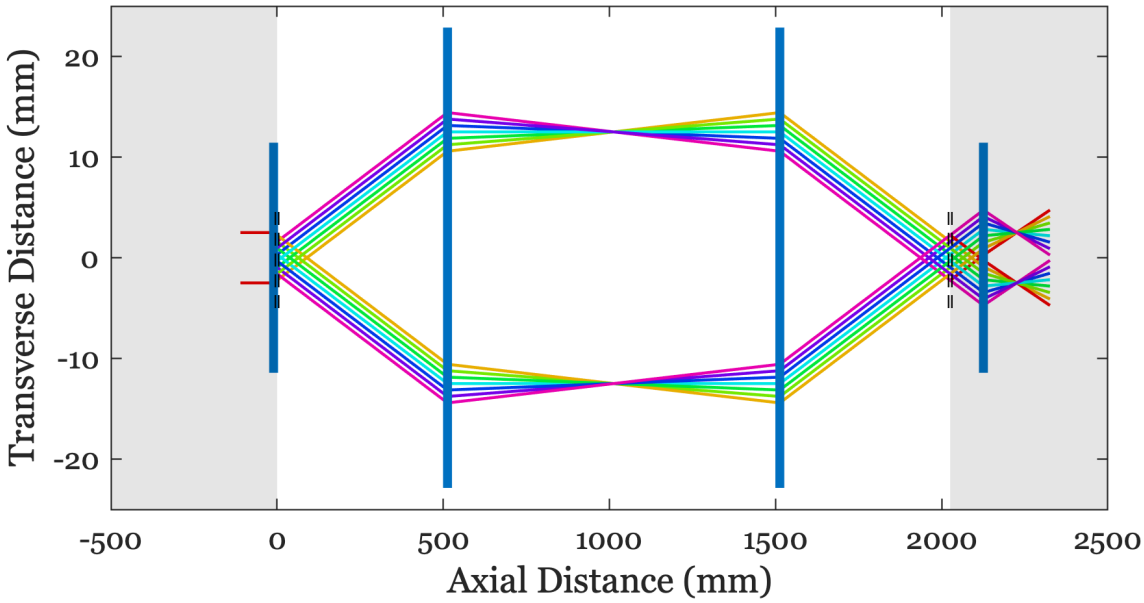

Figure 8. Ray trace of a reverberation loop with beam splitter in image plane.

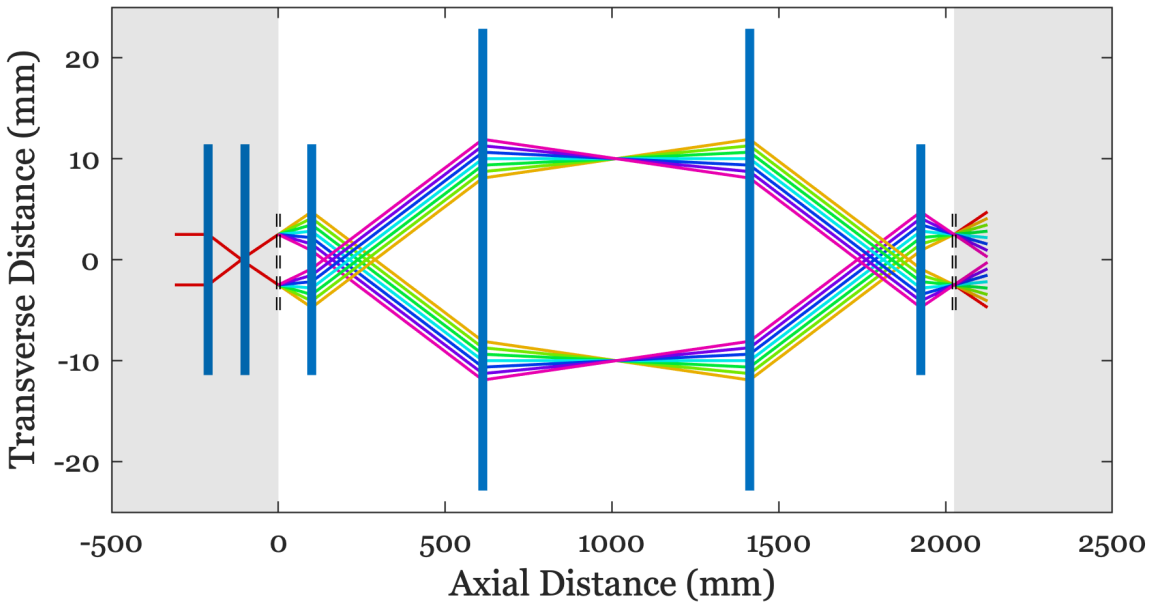

Figure 9. Ray trace of a reverberation loop with beam splitter in pupil plane.

Aberrations

Particular attention must be paid to optical aberrations when designing a reverberation microscope. For shallower planes, the light makes many passes through the reverberation loop which can lead to accumulation of aberrations if set up improperly. Furthermore, while off the shelf optics are optimized for imaging relatively thin surfaces, volumetric imaging as used here involves large axial shifts of the focal spot.

Standard doublet lenses are designed for infinite conjugate ratios – with the object (or focus) one focal length from the lens and the conjugate image at "infinity" on the other side. In reverberation microscopy, the focus is intentionally shifted away from this ideal point (so that the volume can be scanned axially), which unfortunately leads to aberrations. To better understand

this concept, consider the simple 4f relay depicted in Figure 10.

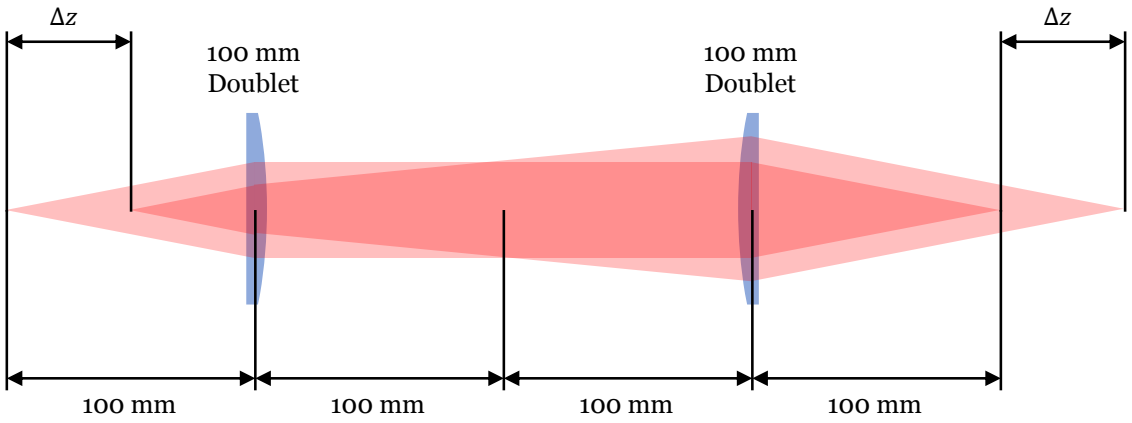

Figure 10. Simple 4f relay with axially shifted focus.

This simple setup consists of a pair of 100 mm doublet lenses configured as a 4f relay, is perfect for characterizing the relationship between axial shift (Δz) and focus quality (Strehl ratio). This is, in effect, a simplified version of what occurs inside the reverberation loop. The magnitude of aberrations were estimated using Zemax OpticStudio, as shown in Figure 11.

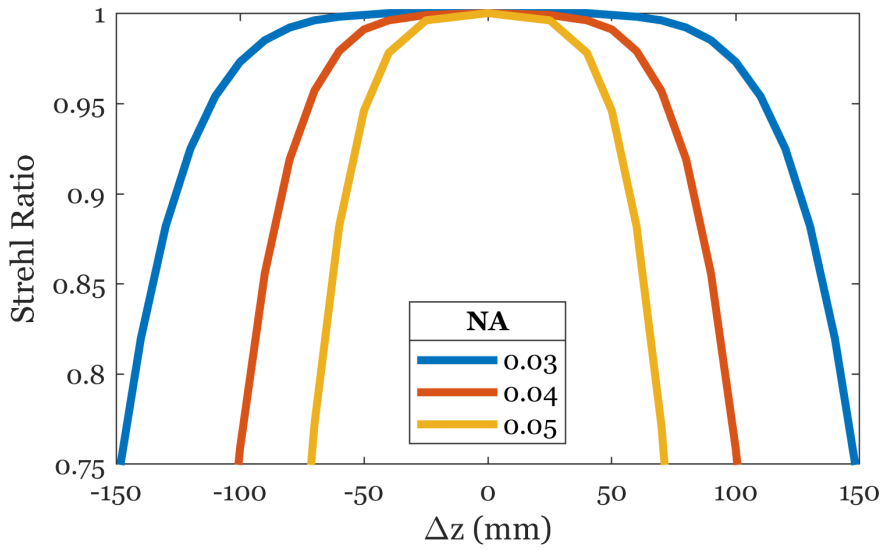

Figure 11. Relationship between axial shift and focus quality.

Near the ideal focus (Δz of 0 mm) the Strehl ratio is essentially 1, indicating diffraction limited performance. In fact, there is a fairly significant margin (approximately ±25 mm) where optical quality remains unaffected. However, once this shift exceeds about ±75 mm, beam quality begins to drop rapidly for higher NAs. It is for this reason that when laying out the reverberation loop, as a rule of thumb, it is preferred to use magnifications and focal lengths which avoid shifting a focus through a lens. This also avoids situations where the laser is focused on the surface or within an optic – also undesirable.

This provides a good feel for how significant aberrations can occur in the reverberation loop; however, it makes sense to extend this analysis more explicitly to the loop as a whole. Figure 12 shows the result of the same analysis applied to the full reverberation loops described in Figure 8 (where the beamsplitter is placed in the image plane) and Figure 9 (where the beamsplitter is placed in the pupil plane).

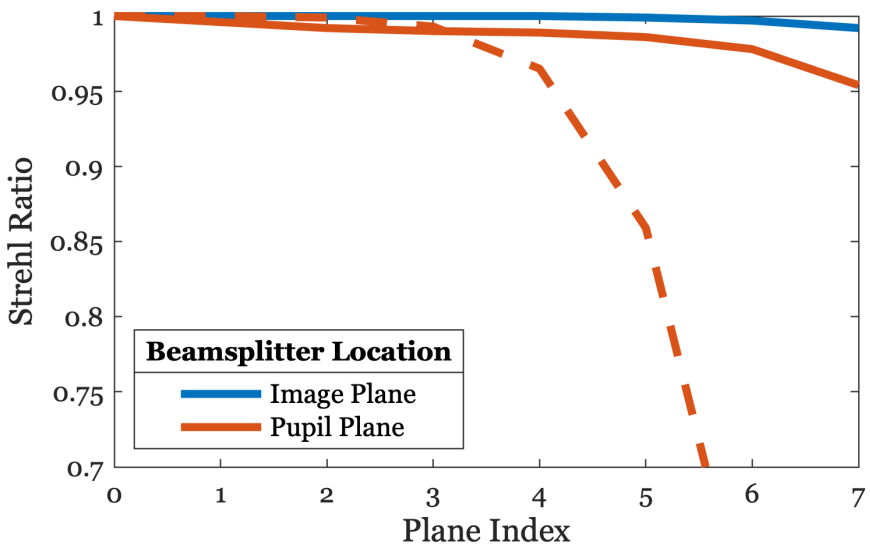

Figure 12. Aberration analysis of the reverberation loops depicted in Figure 8 and Figure 9.

Both designs are able to maintain good beam quality over all eight planes. The dashed line is an excursion case showing what happens when the initial focus isn't shifted before entering the loop (leaving the deepest plane at the nominal focus, rather than centering the set of planes around it). This greatly decreases the useable depth range, only leaving room for four or five planes before the focus moves through a lens in the loop and beam quality drops precipitously.

Dispersion

Dispersion describes the tendency of ultrashort laser pulses (pulse lengths under a picosecond) to spread out in time as they pass through dispersive media (such as the glass of lenses). Dispersive media has a wavelength-dependent speed of light (i.e. the index of refraction changes; see Figure 13). Since pulses are comprised of many wavelengths, some will travel slightly faster than others; the second order effect of this relationship is that a (transform-limited) pulse will

tend to spread out as it travels. The effect is amplified for shorter pulses, which have a wider spread of wavelengths. This is highly relevant to multiphoton microscopy, which specifically utilizes concentrated, short pulses with high peak power to maximize fluorescence generation. (A short pulse generates more multiphoton fluorescence than a longer one with the same total energy.)

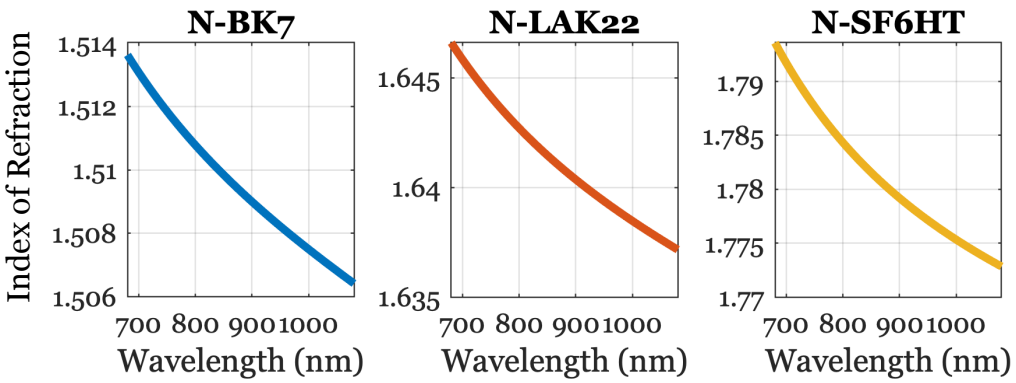

Figure 13. Wavelength dependence of index of refraction for several glasses over Ti:Sapphire laser tuning range.

Dispersion is worth considering in a reverberation microscope design, as the light in the loop passes through many more lenses than would be commonly used. While a basic microscope design may only have 3 lenses (scan, tube, and objective), the reverberation loop can add another 14 or more for the deeper planes (seven passes through a two-lens loop). The impact can be quantified analytically by studying the spread of a gaussian pulse.

The intensity of a gaussian pulse definition can be described as follows, where τ_0 is the pulse length in time and $|z_0|$ is the dispersion length in space ($z_0 = \pi\tau_0^2/D_\nu$) (Saleh 2007, 964):

$$I(z,t) = I_0 \frac{\tau_0}{\tau(z)} \exp\left(-2\frac{\left(t-\frac{z}{v}\right)^2}{\tau(z)^2}\right)$$
$$\tau(z) = \tau_0\sqrt{1+\left(\frac{z}{z_0}\right)^2} = \tau_0\sqrt{1+\left(\frac{D_v z}{\pi\tau_0^2}\right)^2} \quad (13)$$

D_v is the group velocity dispersion (GVD) coefficient, and is material dependent. It is this factor which characterizes the change in pulse width as the pulse propagates ($\tau(z)$), based on the wavelength dependence of the index of refraction (n).

$$D_v = \frac{\lambda_0^3}{c_0^2}\frac{d^2n}{d\lambda_0^2} \quad (14)$$

The GVD for several relevant glasses is plotted in Figure 14.

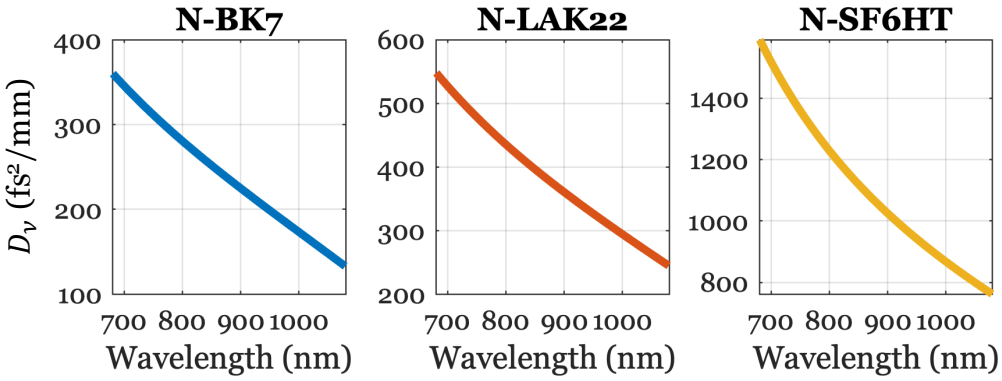

Figure 14. Wavelength dependence of GVD for several glasses over Ti:Sapphire laser tuning range.

For a pulse which travels through multiple materials (with GVD of $D_{v,i}$) of various thicknesses (z_i), the final pulse length (τ) is found by summing the group dispersion delay (GDD, defined as $D_v z$) contributed by each material. Thus $D_v z$ in the second part of equation 13 becomes the total GDD:

$$GDD = \sum_i (GDD)_i = \sum_i D_{v,i} z_i$$
$$\tau = \tau_0 \sqrt{1 + \left(\frac{GDD}{\pi \tau_0^2}\right)^2} \tag{15}$$

Consider the reverberation loop in Figure 5, which contains three dispersive elements. The first is a beam splitter, such as the Thorlabs BS011 (10 mm of N-BK7), giving a GDD of 2,000 fs² at 940 nm. The other two are a pair of relay lenses, such as the Thorlabs AC508-400-B (approximately 4.5 mm of N-LAK22 and 2.6 mm of N-SF6HT), giving a GDD of 4,000 fs² each at 940 nm. This accumulates to about 10,000 fs² of GDD per pass.

For an initial pulse length of 210 fs (that of a Coherent Chameleon Ultra Ti:Sapphire laser[3]), equation 15 gives a final pulse length of 235 fs after seven passes through the loop. This spread is a measurable increase but would not lead to a significant loss of peak power for multiphoton microscopy. Figure 15 shows a parametric plot of this result for a range of wavelengths.

[3] This laser is specified as having a 140 fs long pulse with a sech² shape. To convert this to a comparable gaussian shape (with the same FWHM) for use in equation 15, it must be multiplied by a factor of 1.5. This is how the value of 210 fs is obtained.

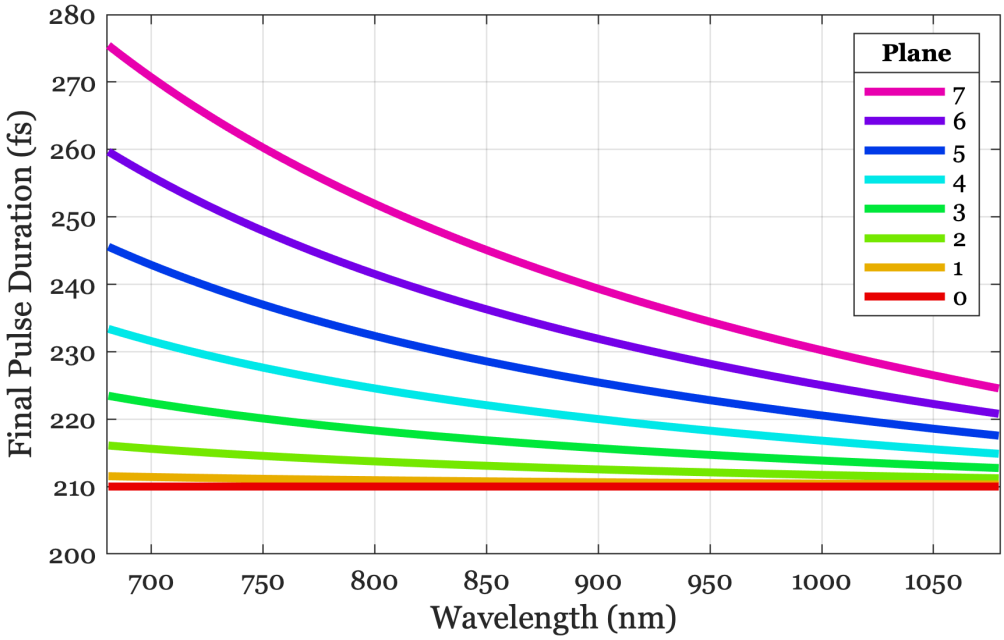

Figure 15. Predicted dispersion caused by reverberation loop over Ti:Sapphire laser tuning range.

POST-PROCESSING TECHNIQUES

Image Processing

The images generated by our reverberation microscopy technique are immediately usable as generated. However, we implemented a few post-processing adjustments to improve image quality, namely crosstalk correction, normalization of intensity, and fine plane alignment.

Simple Crosstalk Correction

There is potential crosstalk between planes if the fluorescence from a previous plane has not fully decayed before the subsequent plane arrives at the detector. This is most prominent for particularly bright features or when the fluorescence lifetime is long relative to the time delay introduced by the loop. A simple method to correct for this effect, is to subtract a proportion (ξ) of each

plane from the subsequent plane. This does require assuming that the detector is linear and that the fluorescence collection efficiency is depth independent. For example, if the fluorescent molecules are assumed to obey single-exponential fluorescence decay statistics of lifetime τ_f, it is readily found that $\xi = \exp(-\tau_r/\tau_f)$ where τ_r is the reverberation time delay.

From an experiment[4] looking at mouse-brain vasculature labeled with FITC, crosstalk was experimentally determined to be approximately $\xi \approx 9\%$ for a $\tau_r \approx 4.7$ ns. From this result, it is inferred that the fluorescence lifetime of FITC is about 2 ns, in accord with the ranges provided previously (Buurman et al. 1992). An example of crosstalk correction is shown in Figure 16, where 9% of the first plane was subtracted from the second, reducing the crosstalk effect.

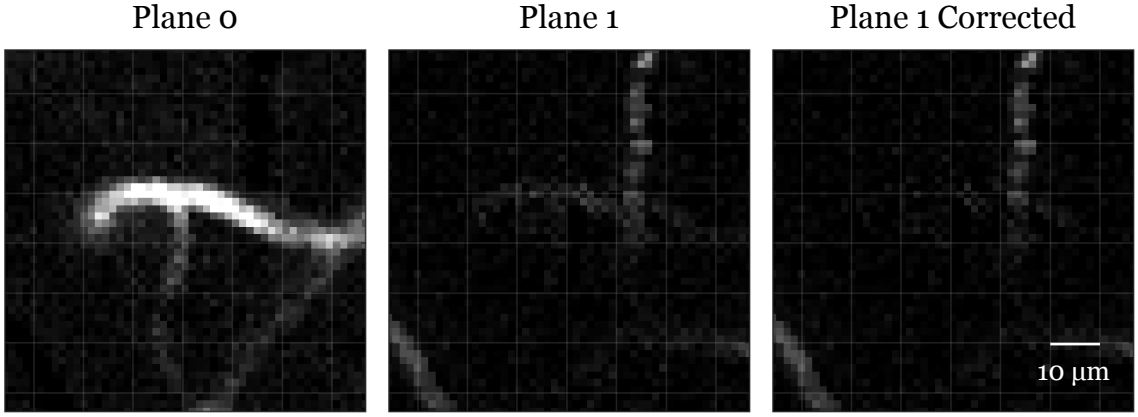

Figure 16. Example of crosstalk removal for mouse-brain vasculature data set.

Image registration is ensured when performing crosstalk subtraction. This is because the crosstalk is entirely caused by residual illumination from the

[4] This result was from one of our earliest designs, which had a reverberation loop length of 1.4 m, hence the relatively short time delay.

previous plane and is thus not affected by, for example, optical misalignment between planes.

Intensity Normalization

While the plane spacing can be set to equilibrate average intensities between planes (i.e. balancing diminished scattering with the diminished power between planes), it may be preferable to use tighter spacing. The side effect is that shallower planes appear dimmer than the deeper ones. This effect is acceptable provided the detector provides sufficient dynamic range. For example, for a given tolerable brightness ratio between the deepest and shallowest planes, the minimum allowed plane spacing Δz_{min} is shown in Figure 17.

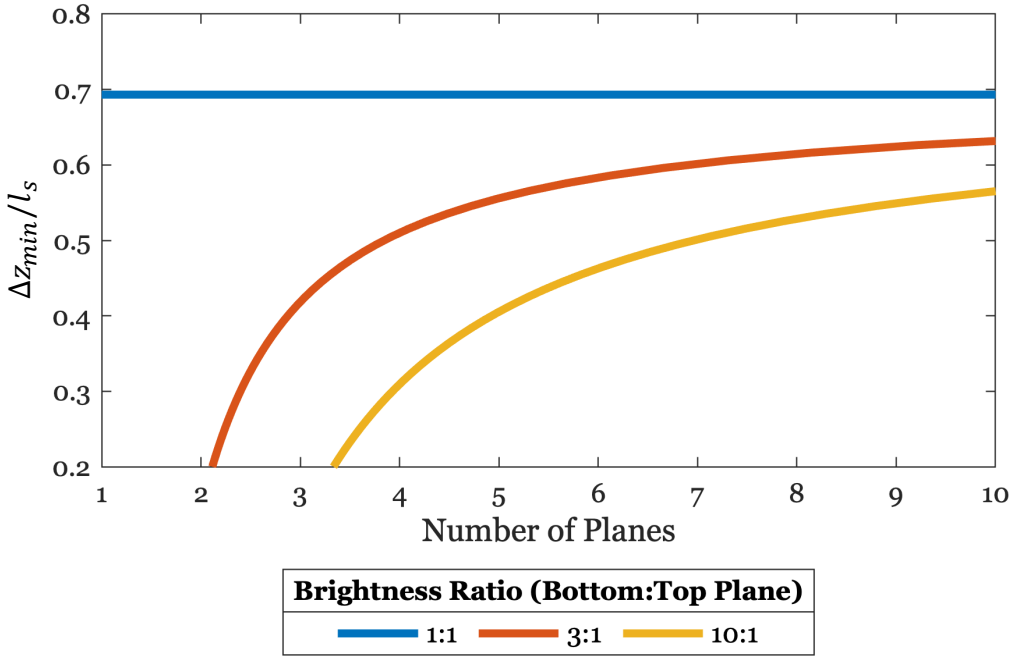

Figure 17. The minimum spacing between planes (normalized to the mean free path).

This intensity scaling is a predictable effect and can be readily corrected numerically. When acquiring image stacks, it may be convenient to normalize the image intensities to the deepest plane (n = 0) in real time. This is achieved by dividing the images from each plane by $\exp[mn(\Delta z/l_s - \ln(s))]$ where m is the multiphoton order (here 2), n is the plane index (here, 0 through 3), and s is the relative incident laser power ratio between planes (nominally 2, from the 50:50 beamsplitter).

Fine Plane Alignment

The final step is to perform a fine alignment of the planes with each other. While it is reasonable to coarsely align the planes by carefully adjusting the mirrors in the reverberation loop, a better fine adjustment can be performed in post processing to handle residual error. To do this, an object is scanned in z to capture an image from each plane at the same depth. The transform between planes (including shift and scale) is found using the MATLAB imregtform function. As this alignment error is an artifact of the optical setup, rather than the sample, it only needs to be determined once at initial setup.

ADVANCED TECHNIQUES

Several additions to the base reverberation technique presented themselves during development. One important aspect of the reverberation approach is that plane separation is tied to scattering of the sample – for typical samples (especially biological tissues) this means plane separation on the order of 100 μm. Deviating too far from this ideal spacing causes the imaging planes to

develop unacceptably large differences in fluorescence intensity. While z-scanning can fill these gaps, this comes with an undesirable speed penalty. Instead, an optical reverberation interleave technique can be used to increase the number of sampling planes with no impact on speed.

Interleaving Reverberation Pulses

The first improvement to the reverberation technique is the implementation of an interleave loop. This secondary loop splits each input pulse in two, seeding a second set of reverberation planes which are interleaved in space and time with the original set. This effectively doubles the number of planes without any speed penalty and, since the two sets are resolved in time, each depth is still measured individually.

To achieve this, the interleave loop is built as a 4-f relay similar to the reverberation loop, but of half the path length. It is introduced with a polarizing beamsplitter just before the primary reverberation loop (see Figure 18); one split leads directly to the reverberation loop (where it seeds a set of planes) while the other first makes a single pass around the interleave loop (before seeding a second set of planes). Since the interleave loop is half the length of the primary loop it introduces half the time delay – achieving the temporal interleave. Likewise, a stage allows shifting the focus of the interleaved seed pulse by half the focal shift of the primary loop – achieving the spatial interleave. A half-wave plate ahead of the beamsplitter controls the relative strength of the primary and interleave loops by rotating the (linear) polarization and adjusting how much

light is initially reflected/transmitted by the beamsplitter. This allows control of the relative power between the primary and interleave planes, however, note that no power is wasted.

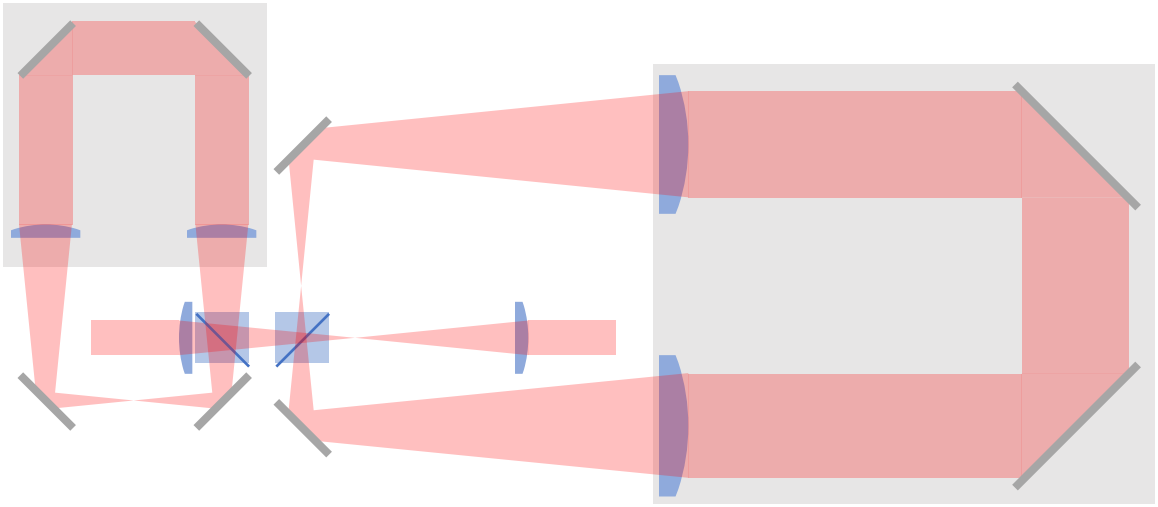

Figure 18. Schematic of interleave loop design.

Volumetric Reverberation Imaging

The interleave loop halves the plane-spacing to 50 µm, however, this is still too large a gap to realize true volumetric imaging. One option for another doubling of planes comes from the use of a piezo objective scanner to quickly take pairs of snapshots at slightly different depths. While normal depth scanning with a piezo is very slow, this is due to the large depths ranges which must be scanned. Here it is only necessary to scan a short distance (25 µm) to fill in between planes. This can be done rapidly – less than 15 ms to scan 25 µm (Figure 19). This enables fully volumetric imaging at video rates (Table 5), albeit with a speed penalty. In practice, one can choose any balance between field of view, plane density, and volume rate to suit the task at hand. This approach is used for

volumetric imaging in the 2PM described in the next chapter.

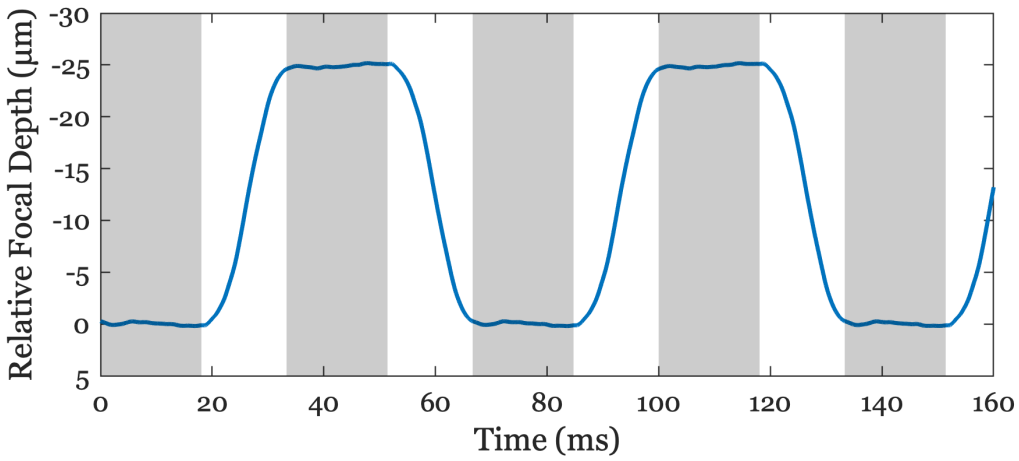

Figure 19. Measured motion of piezo objective scanner operating at 15 Hz.

The mechanical, piezo interleave approach successfully achieves volumetric imaging at video rates. However, it is still a limiting factor for going faster (i.e. approaching 100 Hz). The next level of speed would be to get rid of the piezo interleave and do it all optically with reverberation planes. This could be done simply by adding another interleave loop of half the length of the first. However, this would likely mean increasing the primary reverberation loop (to something on the order of 4 m) in order to keep crosstalk manageable. This would mean three loops, quadrupling layer spacing, for a net of 25 µm plane spacing. While relatively simple on paper, and with few drawbacks optically, it would be somewhat bulky and cumbersome to build in practice.

Advanced Crosstalk Correction

Using a shorter reverberation or interleave loop[5] requires more careful attention to correction of crosstalk between planes. With a short (1 m) loop, planes arrive closely spaced in time (3.3 ns apart) relative to fluorescent lifetime (~4 ns typically) causing significant signal overlap between planes. To achieve a high-quality correction, a deconvolution strategy is used here to separate the planes based on the measured response signal of each plane. Alternatively, it would also be possible to increase the loop lengths to avoid significant overlap altogether, but this comes at the cost of increasing the physical size of the microscope and optics.

A single-layer bead sample is used to measure the fluorescent response (in time) of each reverberation individually (Figure 20). These measurements allow us to build a c×n response matrix (where c is the number of measurement channels, and n is the number of planes), R, which maps the n×1 source fluorescence, f, to c×1 measured signal $m = Rf$.

[5] For example, the interleave loop in our 2PM design is 1 m long and leads to quite a bit of crosstalk between planes. We found the simple crosstalk approach from the previous chapter no longer provided the level of correction we desired.

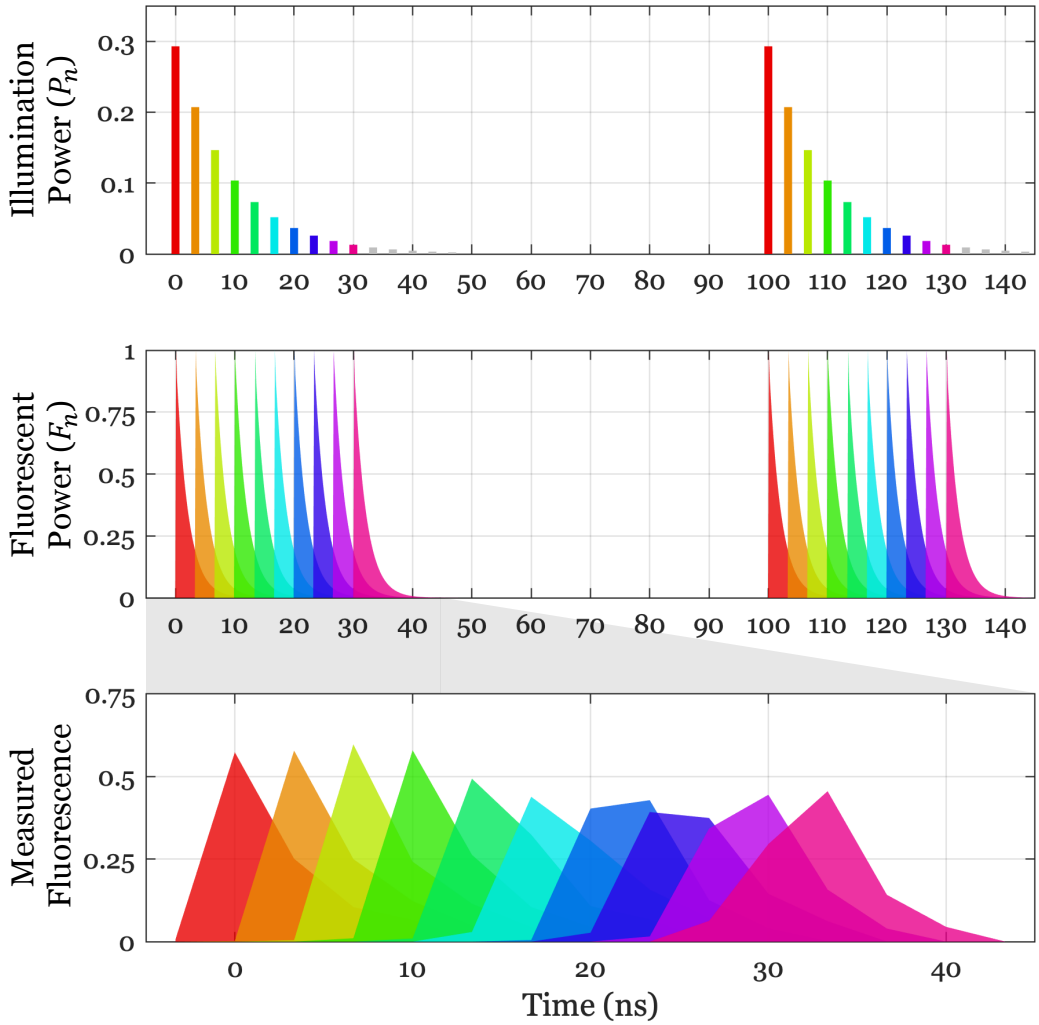

Figure 20. Timeline of signal pulses for each plane – top: illumination pulse intensity, middle: idealized fluorescence intensity, bottom: measured fluorescence intensity.

In operation, the measured value across the channels can then be used to reconstruct the source fluorescence using a reconstruction matrix, R^{-1}, $f = R^{-1}m$. This operation is fast enough to be performed in real time, and accounts for all details of the response shape. The drawback is that it is assumed the sample has a similar fluorescence lifetime to the calibration beads. Note that while it may be possible to predict the response instead of measuring it, there are

many conflating factors (fluorescence lifetime, recording bandwidth, sampling rate, loop delay, and so on) which make such an approach non-trivial.

MICROSCOPE HARDWARE

The prototype microscope designs used to develop the reverberation technique were iteratively improved throughout the course of research. As such, many aspects of the setup changed significantly over time. What follows below is a description of the final configuration (as of this writing) of both the two and three photon reverberation microscopes. Any noteworthy influence on experimental results due to these design modifications will be noted in the results section as necessary.

Figure 21 shows a schematic of the reverberation microscope design. Both two and three photon setups have the same overall design, however the three photon lacks an interleave loop. Numbered elements in the primary optical path correspond to the parts lists in the following sections.

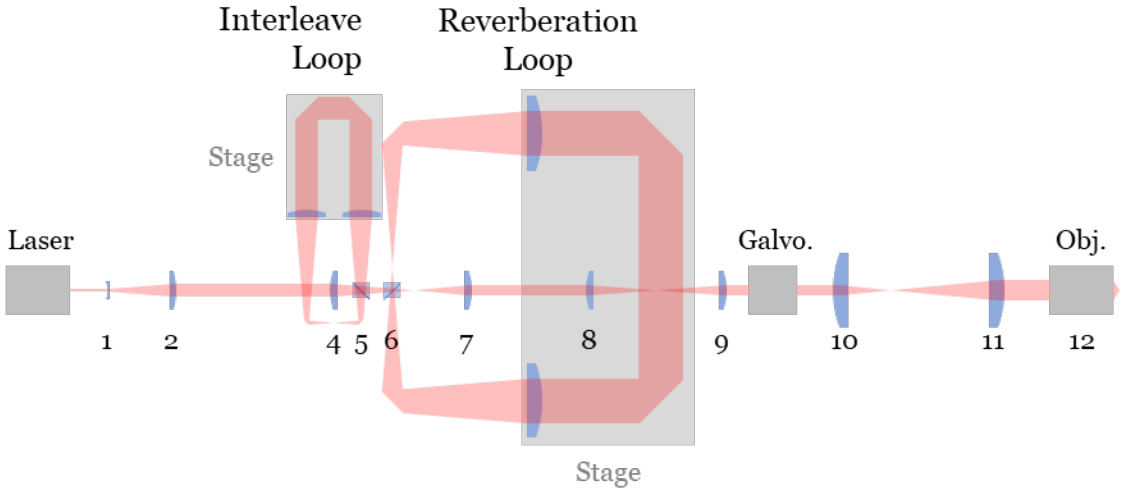

Figure 21. Schematic of reverberation microscope with interleave.

Two Photon Microscope

The 2PM is designed with a primary 2 m reverberation loop (a pair of Thorlabs AC508-500-B-ML 500 mm lenses), as well as a secondary 1m loop (a pair of Thorlabs AC508-250-B-ML 250 mm lenses) for optically interleaving a second set of planes. Another (mechanical) interleave is provided by an nPoint nPFocus100 objective scanner. The front end of the microscope is essentially a standard scanning microscope, with the reverberation components introduced before the beam steering galvanometers. The components in the primary optical path are listed sequentially in Table 3.

#	Component	Thorlabs Part #	Note
1	-30 mm lens	LC1060-B-ML	5× beam expander
2	150 mm lens	AC254-150-B-ML	
3	Half wave plate	AHWP10M-980	Polarization rotator
4	150 mm lens	AC254-150-B-ML	Depth controller
5	Polarized beamsplitter	PBS103	Interleave loop entry
6	50:50 beamsplitter	BS011	Reverberation loop entry
7	100 mm lens	AC254-100-B-ML	1× relay
8	125 mm lens	AC254-125-B-ML	
9	125 mm lens	AC254-125-B-ML	
10	93 mm lens (equiv.)	n/a	2.1× scan/tube lens
11	200 mm lens (equiv.)	n/a	
12	12.5 mm objective	N16XLWD-PF	

Table 3. Optical components in 2PM primary path, ordered sequentially.

A beam expander (#1-2) enlarges the laser beam to achieve the desired final beam size (and therefore resolution). A half wave plate (#3) is used to rotate polarization, setting the relative power between primary reverberation planes and interleave planes. A lens relay (#4, 7) creates the focal space where the loops are introduced by beamsplitters (#5, 6). Moving lens #4 axially changes the depth of

the deepest plane, allowing the set of planes to remain centered around the microscope's optimal focus. Lens #4 has a longer focal length than #7 only for the practical purpose of creating enough space to fit both beamsplitters. (The magnification incidentally introduced is compensated by the beam expander.) The entirely assembly (#3-7) can be slid in and out of place to switch between normal and reverberation imaging modes.

The 1× relay (#8-9) not optically necessary and is simply for the practical purpose of relaying the pupil plane from the optical table surface to the top of the microscope and into the scanning mirrors. The scan and tube lenses (#10-11) are actually a more complex optical component designed by Thorlabs, but in practice is simply equivalent 2.1× relay with low aberration. Finally, the objective is a Nikon CFI75 LWD 16× with a numerical aperture of 0.8.

The 2PM is equipped with two lasers: a Coherent Chameleon Ultra II (80 MHz repetition rate) with highest power (>2 W) in a tunable wavelength range (700-950 nm) best for green fluorescent markers, and a Coherent Fidelity (10 W power, 10 MHz repetition rate) with fixed wavelength (1040 nm) best suited for red fluorescent markers. These are configured to operate separately (with manual changeover via a flip mirror and switching cables), but there is no technical reason they could not be merged with a dichroic beamsplitter for simultaneous two-color reverberation imaging.

The Chameleon laser has it's 80 MHz pulse rate reduced to 20 MHz by a Conoptics pulse picker (Model 350-210-RA) to provide sufficient time between

pulses for readout of reverberation planes. Beam steering is performed with a Thorlabs LSK-GR08 galvo-resonant scan head. Detection is performed by a Hamamatsu Hamamatsu R11322U-40 hybrid photodetector, amplified by a Femto HCA-400M-5K-C. Readout is performed by a National Instruments 5771 digitizer and 7972 FPGA combination using customized Vidrio ScanImage software. An Analog Devices AD9516 is used to synchronize the digitizer sampling to the laser pulses. The instrument response time of the detection electronics is confirmed to be better than a nanosecond, as inferred from the signal produced by a second-harmonic crystal sample. This setup is summarized in Table 4.

Laser (green)	Coherent Chameleon Ultra II
Laser (red)	Coherent Fidelity
Electro-optic modulator	Conoptics 350-210-RA
Resonant galvanometer	Thorlabs LSK-GR08
Clock generator	Analog Devices AD9516-1
Sensor (HPD)	Hamamatsu R11322U-40
Objective scanner	nPoint nPFocus100
Amplifier	Femto HCA-400M-5K-C
Digitizer	National Instruments 5771
FPGA	National Instruments 7972
Software	Vidrio ScanImage (Custom)

Table 4. Other components in 2PM.

Some imaging modes for this microscope are listed in Table 5. The field of view is limited to a 760 μm × 760 μm region by vignetting in the scan/tube lens. For this table, the pixels are sized to match a 1.8 μm fluorescent spot size (with 25 μm thickness). Two volume rates are given, one for volumetric imaging (which uses both the mechanical and optical interleave) and one for fast multi-plane imaging (which leaves gaps, but only uses optical interleave).

Zoom	FOV (μm)	Resolution (px)	Volume Rate (Hz)	
			Volumetric[a]	Multi-Plane[b]
1×	760	422	12	36
2×	380	211	18	70
4×	190	106	23	130

[a]25 μm plane separation, [b]50 μm plane separation

Table 5. Sample of 2PM imaging modes.

Three Photon Microscope

The 3PM is designed with only a primary 2 m reverberation loop (a pair of Thorlabs AC508-500-C-ML 500 mm lenses). It does not have the optical or mechanical interleave capabilities, but they could be trivially added. The front end is again essentially a standard scanning microscope, with the reverberation components introduced before the beam steering galvanometers. The components in the primary optical path are listed sequentially in Table 6.

#	Component	Thorlabs Part #	Note
1	-25 mm lens	LC1054-C-ML	3× beam expander
2	75 mm lens	AC127-075-C-ML	
3	-	-	
4	100 mm lens	AC254-100-C-ML	Depth controller
5	-	-	
6	50:50 beamsplitter	BS012	Reverberation loop entry
7	100 mm lens	AC254-100-C-ML	
8	125 mm lens	AC254-125-C	1× relay
9	125 mm lens	AC254-125-C	
10	110 mm lens	LSM05	1.8× scan/tube lens
11	200 mm lens	TL200-3P	
12	12.5 mm objective	N16XLWD-PF	

Table 6. Optical components in 3PM primary path, ordered sequentially.

The 3PM is equipped with a Coherent Opera-F (2 W power, 1 MHz repetition rate) pumped by a Coherent Monaco. Due to the low repetition rate, a scanning galvanometer (Thorlabs GVS002) is used instead of the resonant one in

the 2PM. The remainder of the components (summarized in Table 7) are essentially equivalent to the 2PM, except for the lack of an objective scanner for piezo interleave.

Laser (pump)	Coherent Opera-F
Optical parametric amplifier	Coherent Monaco
Scanning galvanometer	Thorlabs GVS002
Clock generator	Analog Devices AD9516-0
Sensor (HPD)	Hamamatsu R11322U-40
Amplifier	Femto HCA-400M-5K-C
Digitizer	National Instruments 5771
FPGA	National Instruments 7972
Software	Vidrio ScanImage (Custom)

Table 7. Other components in 3PM.

Some imaging modes for this microscope are listed in Table 6. For this microscope, volume rate is limited by the 1 MHz laser repetition rate rather than the galvanometer scan speed. The rates in the table assume a requirement of two pulses per pixel on average.

			Volume Rate (Hz)	
Zoom	**FOV (μm)**	**Resolution (px)**	**Volumetric[a]**	**Multi-Plane[b]**
1×	1000	500	n/a	2
2×	500	250	n/a	8
4×	250	125	n/a	32

[a]Interleave not installed, [b]100 μm plane separation

Table 8. Sample of 3PM imaging modes.

Alignment Technique

The reverberation loop is a somewhat unusual component for a microscope, and so it may not be readily apparent how to align it to the rest of the system. A useful alignment process for a reverberation loop with the beamsplitter in the image plane proceeds as follows, referring to the lenses (L) and mirrors (M) of Figure 22.

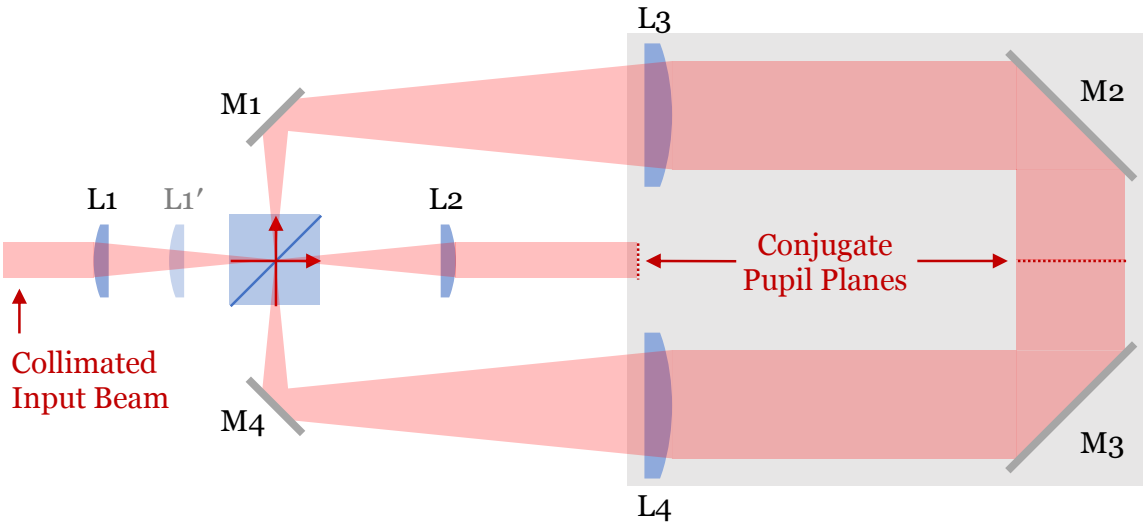

Figure 22. Diagram for alignment of reverberation loop.

Firstly, the microscope itself (without any reverberation loop) should be aligned using standard techniques. The loop can then be incorporated by moving L1, L2, and the beamsplitter into place. Done properly, these should have no net effect on beam alignment. L1 can be translated axially (to L1′ for example) to set the depth of the deepest plane, however, L2 should always be precisely one focal length from a pupil plane. A coarse alignment of the loop can then be performed by adjusting the mirrors in sequence. Use M1 to center the beam on L3, M2 to center on M3, M3 on L4, and finally M4 onto the center of the beamsplitter.

Next, an iterative process, alternating between image and pupil planes, is used for a finer alignment. Several focal spots should be evident just past the beamsplitter (outside the loop). Alternate between M3 and M2, using M3 to center the focal spots on each other, while using M2 to keep the beam centered on L4. Several pupil spots should also be evident near the pupil plane (outside the loop). Alternate between M1 and M4, using M4 to center the pupil spots on

each other, while using M1 to keep the beam centered on L3. Several iterations, switching between focal and pupil spots, may be necessary before the alignment converges.

EXPERIMENTAL RESULTS

Fluorescent Beads

Initial testing and characterization of reverberation MPM was done with 10 μm fluorescent beads embedded in a scattering medium with l_s of approximately 100 μm (Beaulieu et al. 2018). A single-shot reverberation image taken at a depth of 225 μm, consisting of four planes spaced 68 μm apart, is shown in the top row of Figure 23, Additionally, Figure 23 shows x-z slices obtained from each plane as the sample was vertically scanned by a stage from the surface to 250 μm. The shallower depths, which were separately imaged in different reverberation planes during the extended z-scan, generated the same result with comparable image quality regardless of which plane was used.

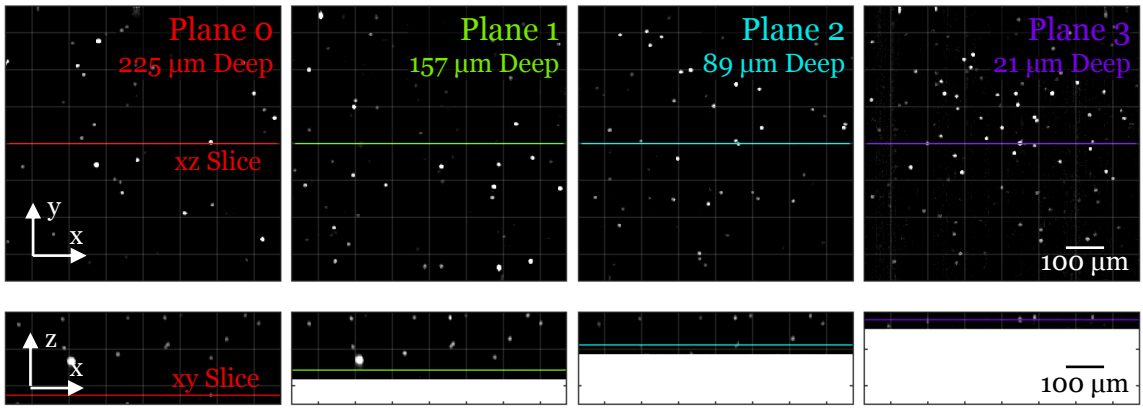

Figure 23. Characterization of reverberation MPM with 10 μm fluorescent beads in thick, scattering media.

Profiles of the transverse and axial responses for a single bead are shown in Figure 24, demonstrating that a reverberation microscope provides 3D micron-scale resolution similar to a conventional MPM, with a point spread function that is not significantly modified between planes.

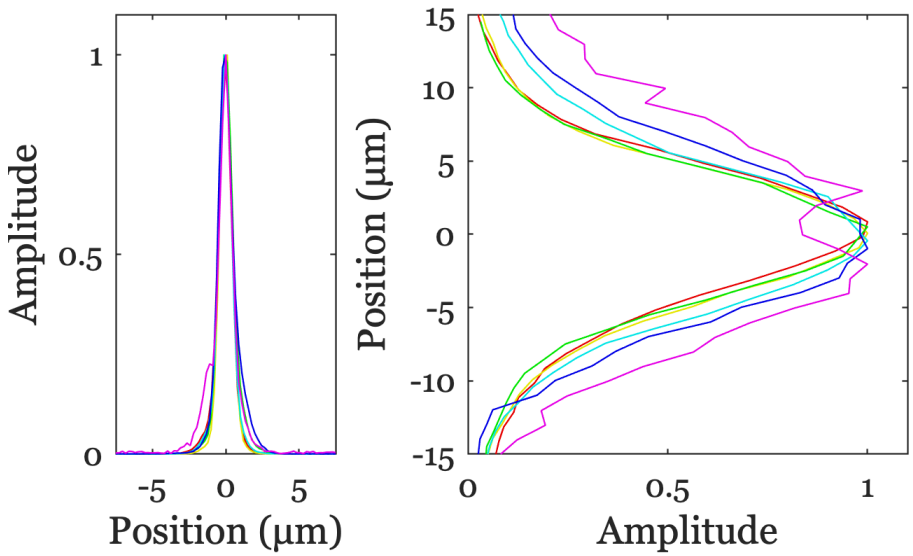

Figure 24. Transverse and axial point spread functions for first six planes, as measured with a 1 μm bead.

A final bead data set is a volumetric reverberation image, using both pulse- and piezo-interleave techniques to achieve volumetric data at video rates, shown in Figure 25. This figure is a single frame from a video collected at 15 Hz.

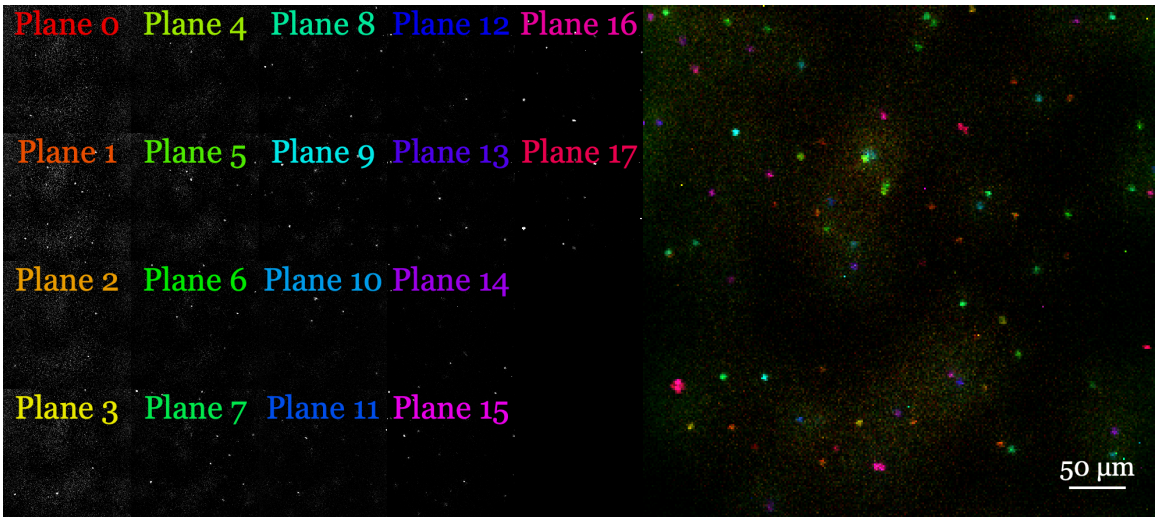

Figure 25. Volumetric reverberation MPM image of scattering bead sample.

In-Vivo Mouse-Brain Vasculature

In-vivo imaging of mouse-brain vasculature labeled with FITC-Dextran (Figure 26) demonstrates the effectiveness of reverberation MPM for biological imaging (Beaulieu et al. 2020). In this experiment l_s was found to be approximately 200 µm for a two photon excitation wavelength of 940 nm, and the planes were spaced 92 µm apart. The six independent planes are shown across the top of the figure, with a merged image in the bottom left. Color indicates plane/depth (the single color of each plane merged in overlapping regions). Finally, in the bottom right, there is a maximum intensity projection of a z-stack (using short physical z-scan to fill in the gaps between reverberation planes) with slices from all six reverberation planes merged into a volume. The highlighted planes correspond to the single shot shown in the rest of the figure.

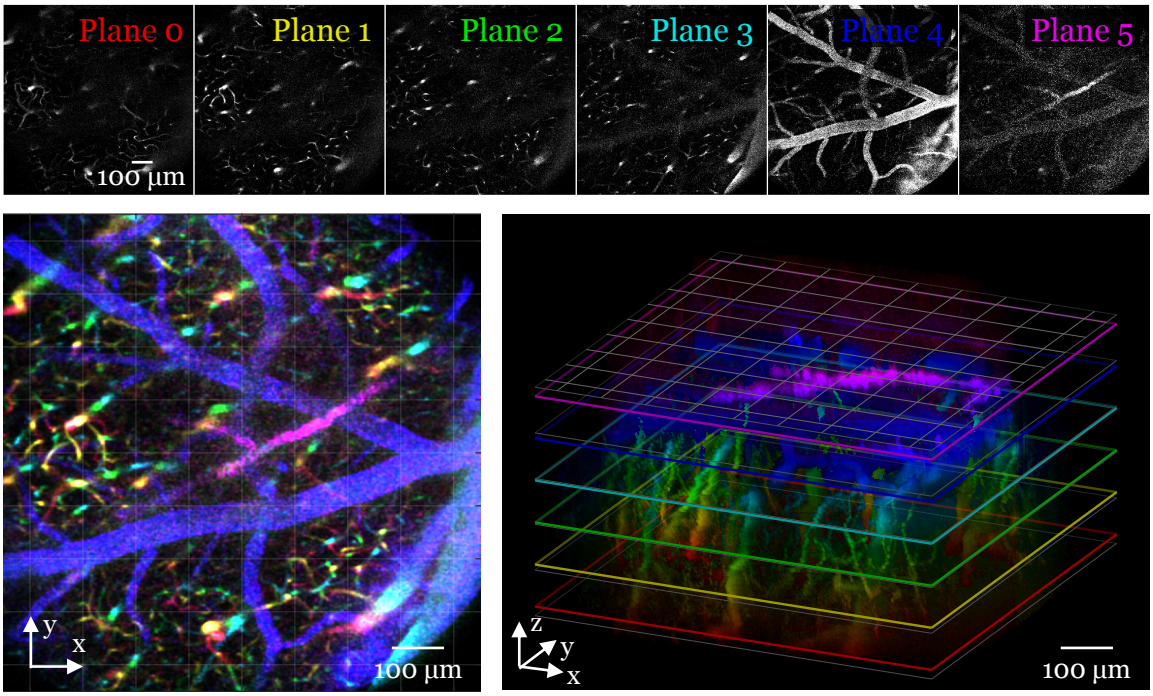

Figure 26. Reverberation 2PM imaging of in-vivo mouse-brain vasculature.

These results illustrate the capacity of reverberation microscopy to obtain a comprehensive snapshot of brain tissue over an extended depth range, acquired as multiple independent, optically sectioned planes spanning large fields of view (here up to 900 µm).

In-Vivo Mouse-Brain Neural Activity

Ca^{2+} imaging of GCaMP6-labelled neurons in the mouse motor cortex and olfactory bulb demonstrates the ability of reverberation MPM to image dynamic samples at video rates (Beaulieu et al. 2020). Both resting activity and sensory-driven responses are clearly visible across several imaging planes, illustrating the ability to simultaneously monitor neural activity over multiple cell layers. These

data sets were taken with the 2PM without any interleaved planes.[6]

Figure 27 shows time-averaged XY images of GCaMP6s-expressing neurons from four different planes of neocortex, with the top plane positioned at the brain surface. Traces to the right show activity of individual neurons imaged in different sub-surface layers.

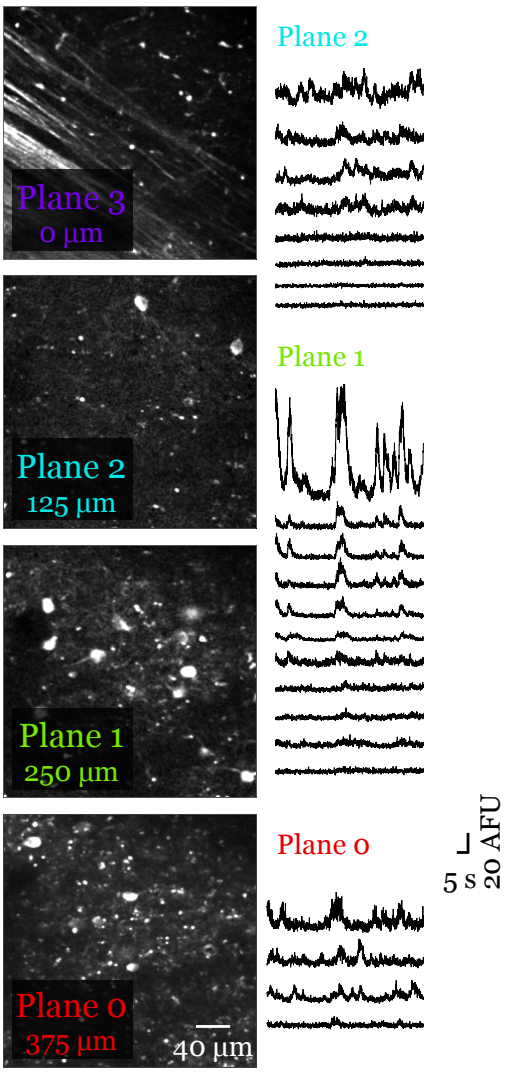

Figure 27. Reverberation imaging of GCaMP6s-expressing neurons from four different planes of neocortex.

[6] We simply hadn't implemented the interleave at the time of these experiments.

Figure 28 shows time-averaged XY images of dendrites and somata of GCaMP6f-expressing neurons imaged in three different planes of main olfactory bulb. To the right, representative traces show sensory responses to the odorant ethyl tiglate in postsynaptic dendrites (gold) and somata of two different classes of OB projection neurons (blue, green).

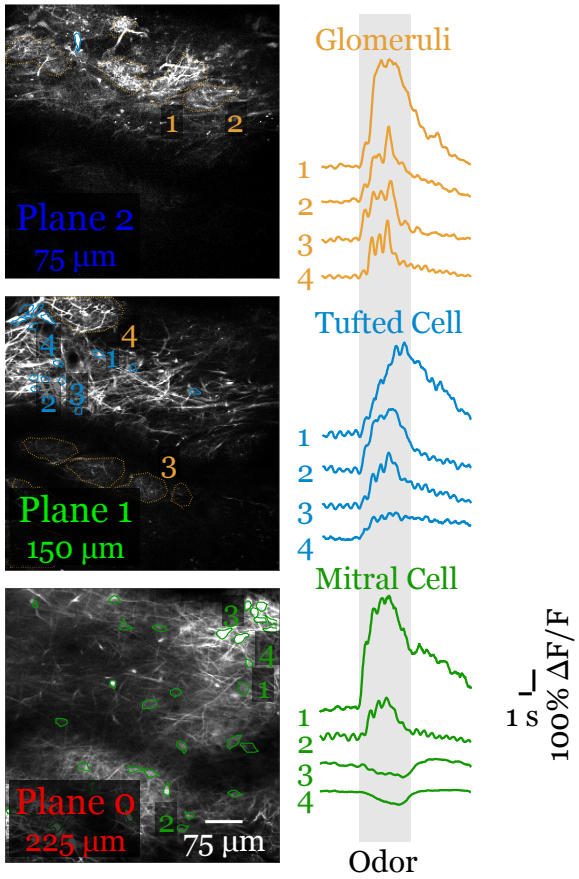

Figure 28. Reverberation imaging of dendrites and somata of GCaMP6f-expressing neurons imaged from three different planes of main olfactory bulb.

The multiplane imaging rate provided by the microscope is limited by the speed of transverse x-y scanning, which here is video-rate (30 Hz) and thus amply sufficient to monitor even the fastest GCaMP6 dynamics.

Cardiac Tissue

The final type of sample tested is cardiac tissue, which has scattering properties similar to that of the brain tissue from the previous section. Reverberation microscopy is of particular interest for this application as there is interest amongst tissue engineers to image structures within living, beating, lab-grown heart samples. Widefield microscopes cannot penetrate the scattering, while traditional techniques (confocal or regular multiphoton microscopy) cannot handle the movement of the tissue – the cells tend to move in and out of the thin image plane and cannot be tracked through the entire movement. Reverberation microscopy solves both these problems, by imaging a large volume at high speed.

Early, demonstration experiments on fixed tissue are shown in Figure 29. Here, the entire, balloon-shaped sample is labeled (f-actin of all cells labeled with Alexa Fluor 647) and imaged with four reverberation planes extending several hundred microns below the surface.

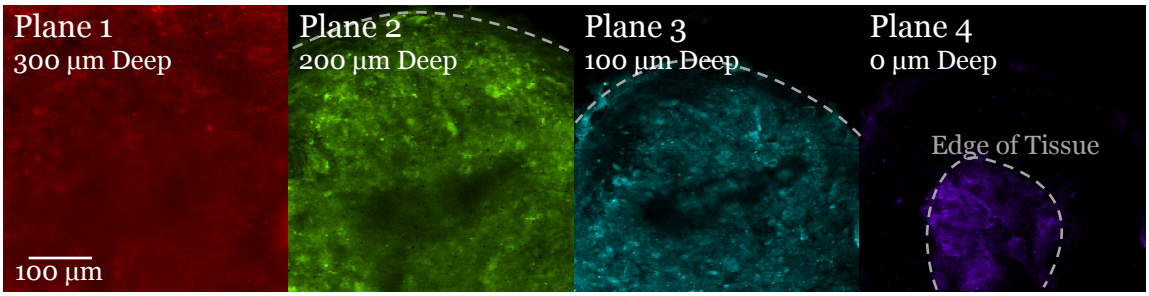

Figure 29. Reverberation image of fixed cardiac tissue sample.

These experiments continued with the vascularized tissue shown in Figure 30. (While this particular image comes from a fixed sample, identical experiments have been performed on live tissues.) Here volumetric reverberation

is used at 15 Hz, with 25 μm spacing between planes. Such video rate imaging allows recording as the tissues move without loss of resolution.

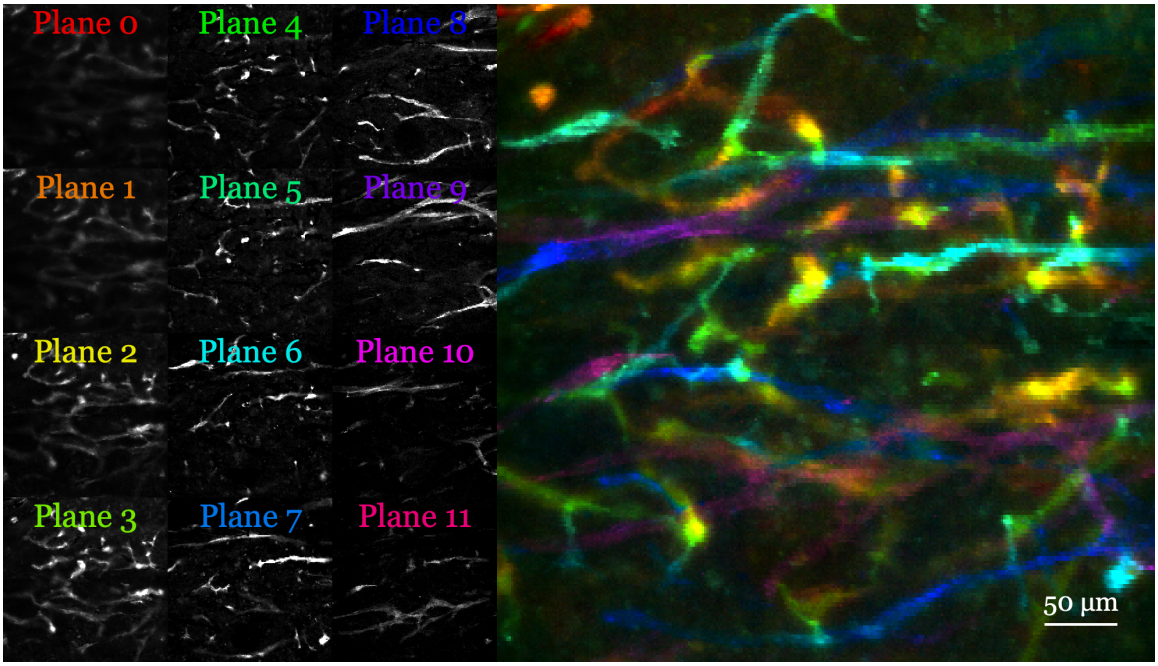

Figure 30. Volumetric reverberation image of vasculature in cardiac tissue sample.

CONCLUSIONS

Reverberation MPM presents many advantages for multiplane and volumetric imaging, with few drawbacks. By splitting each laser pulse into a continuous series of beam foci, multiple planes can be probed near-simultaneously from a large depth (in principle arbitrary) all the way to the sample surface. In cases where depth penetration is laser-power limited, the price paid is a small reduction in the maximum attainable depth penetration by an amount Δz. Reverberation MPM is both light efficient and simple to implement, requiring only the addition of a reverberation loop to a conventional MPM equipped with fast detection electronics. Addition of a supplemental interleave

loop takes the technique even further, increasing plane density and enabling high resolution imaging of full volumes. These advantages make it particularly attractive as a general technique for fast, high resolution, large-scale volumetric imaging in scattering media.

BIBLIOGRAPHY

Amir, W, R Carriles, E E Hoover, T a Planchon, C G Durfee, and J a Squier. 2007. "Simultaneous Imaging of Multiple Focal Planes Using a Two-Photon Scanning Microscope." *Optics Letters* 32 (12): 1731–1733.

Beaulieu, Devin R., Ian G. Davison, Thomas G. Bifano, and Jerome Mertz. 2018. "Simultaneous Multiplane Imaging with Reverberation Multiphoton Microscopy." *ArXiv:1812.05162 [Physics]*, December. http://arxiv.org/abs/1812.05162.

Beaulieu, Devin R., Ian G. Davison, Kıvılcım Kılıç, Thomas G. Bifano, and Jerome Mertz. 2020. "Simultaneous Multiplane Imaging with Reverberation Two-Photon Microscopy." *Nature Methods*, February. https://doi.org/10.1038/s41592-019-0728-9.

Beaurepaire, E, M Oheim, and J Mertz. 2002. "Ultra-Deep Two-Photon Fluorescence Excitation in Turbid Media." *Optics Communications*, 41 (25): 5376–5382. https://doi.org/10.1364/AO.41.005376.

Berezin, Mikhail Y., and Samuel Achilefu. 2010. "Fluorescence Lifetime Measurements and Biological Imaging." *Chemical Reviews* 110 (5): 2641–84. https://doi.org/10.1021/cr900343z.

Buurman, E. P., R. Sanders, A. Draaijer, H. C. Gerritsen, J. J. F. van Veen, P. M. Houpt, and Y. K. Levine. 1992. "Fluorescence Lifetime Imaging Using a Confocal Laser Scanning Microscope." *Scanning* 14 (3): 155–159. https://doi.org/10.1002/sca.4950140305.

Chen, Jerry L, Fabian F Voigt, Mitra Javadzadeh, Roland Krueppel, and Fritjof Helmchen. 2016. "Long-Range Population Dynamics of Anatomically Defined Neocortical Networks." *ELife* 5 (May). https://doi.org/10.7554/eLife.14679.

Cheng, Adrian, J Tiago Gonçalves, Peyman Golshani, Katsushi Arisaka, and Carlos Portera-Cailliau. 2011. "Simultaneous Two-Photon Calcium Imaging at Different Depths with Spatiotemporal Multiplexing." *Nature Methods* 8 (2): 139–142. https://doi.org/10.1038/nmeth.1552.

Grewe, Benjamin F, Fabian F Voigt, Marcel van 't Hoff, and Fritjof Helmchen. 2011. "Fast Two-Layer Two-Photon Imaging of Neuronal Cell Populations Using an Electrically Tunable Lens." *Biomedical Optics Express* 2 (7): 2035–2046. https://doi.org/10.1364/BOE.2.002035.

Helmchen, Fritjof, and Winfried Denk. 2005. “Deep Tissue Two-Photon Microscopy.” *Nature Methods* 2 (12): 932–940. https://doi.org/10.1038/nmeth818.

Heshmat, Barmak, Matthew Tancik, Guy Satat, and Ramesh Raskar. 2018. “Photography Optics in the Time Dimension.” *Nature Photonics* 12 (9): 560–566. https://doi.org/10.1038/s41566-018-0234-0.

Horton, Nicholas G., Ke Wang, Demirhan Kobat, Catharine G. Clark, Frank W. Wise, Chris B. Schaffer, and Chris Xu. 2013. “In Vivo Three-Photon Microscopy of Subcortical Structures within an Intact Mouse Brain.” *Nature Photonics* 7 (3): 205–209. https://doi.org/10.1038/nphoton.2012.336.

Hu, Qinglei, Pei Li, Yumiao Xiong, Yu Wang, Xiaohua Lv, and Shaoqun Zeng. 2018. “Simultaneous Two-Plane, Two-Photon Imaging Based on Spatial Multiplexing.” *Optics Letters* 43 (19): 4598. https://doi.org/10.1364/OL.43.004598.

Ji, Na, Jeremy Freeman, and Spencer L Smith. 2016. “Technologies for Imaging Neural Activity in Large Volumes.” *Nature Neuroscience* 19 (9): 1154–64. https://doi.org/10.1038/nn.4358.

Kong, Lingjie, Jianyong Tang, Justin P Little, Yang Yu, Tim Lämmermann, Charles P Lin, Ronald N Germain, and Meng Cui. 2015. “Continuous Volumetric Imaging via an Optical Phase-Locked Ultrasound Lens.” *Nature Methods* 12 (8): 759–762. https://doi.org/10.1038/nmeth.3476.

Lu, R, W Sun, Y Liang, A Kerlin, J Bierfeld, J D Seelig, D E Wilson, et al. 2017. “Video-Rate Volumetric Functional Imaging of the Brain at Synaptic Resolution.” *Nature Neuroscience* 20: 620.

Olivier, Nicolas, Alexandre Mermillod-Blondin, Craig B. Arnold, and Emmanuel Beaurepaire. 2009. “Two-Photon Microscopy with Simultaneous Standard and Extended Depth of Field Using a Tunable Acoustic Gradient-Index Lens.” *Optics Letters* 34 (11): 1684. https://doi.org/10.1364/OL.34.001684.

Prevedel, Robert, Aart J. Verhoef, Alejandro J. Pernía-Andrade, Siegfried Weisenburger, Ben S. Huang, Tobias Nöbauer, Alma Fernández, et al. 2016. “Fast Volumetric Calcium Imaging across Multiple Cortical Layers Using Sculpted Light.” *Nature Methods* 13 (12): 1021–1028. https://doi.org/10.1038/nmeth.4040.

Saleh, Bahaa E. A. 2007. *Fundamentals of Photonics*. 2nd ed.. Hoboken, N.J.: Hoboken, N.J. : Wiley-Interscience.

Shain, William J., Nicholas A. Vickers, Bennett B. Goldberg, Thomas Bifano, and Jerome Mertz. 2017. "Extended Depth-of-Field Microscopy with a High-Speed Deformable Mirror." *Optics Letters* 42 (5): 995. https://doi.org/10.1364/OL.42.000995.

Sofroniew, N. J., D. Flickinger, J. King, and K. Svoboda. 2016. "A Large Field of View Two-Photon Mesoscope with Subcellular Resolution for in Vivo Imaging." *ELife* 5: e14472.

Song, A., A. S. Charles, S. A. Koay, J. L. Gauthier, S. Y. Thiberge, J. W. Pillow, and D. W. Tank. 2017. "Volumetric Two-Photon Imaging of Neurons Using Stereoscopy (VTwINS)." *Nature Methods* 14: 420–426.

Stirman, J. N., I. T. Smith, M. W. Kudenov, and S. L. Smith. 2016. "Wide Field-of-View, Multi-Region, Two-Photon Imaging of Neuronal Activity in the Mammalian Brain." *Nature Biotechnology* 34 (8): 857–862.

Theer, Patrick, Mazahir T Hasan, and Winfried Denk. 2003. "Two-Photon Imaging to a Depth of 1000 Mm in Living Brains by Use of a Ti:Al2O3 Regenerative Amplifier," *Optics Letters* 28 (12): 1022–1024. https://doi.org/10.1364/OL.28.001022.

Theriault, G, Y. De Koninck, and N. McCarthy. 2013. "Extended Depth of Field Microscopy for Rapid Volumetric Two-Photon Imaging." *Optics Express* 21: 10095.

Yang, Weijian, Jae eun Kang Miller, Luis Carrillo-Reid, Eftychios Pnevmatikakis, Liam Paninski, Rafael Yuste, and Darcy S. Peterka. 2015. "Simultaneous Multi-Plane Imaging of Neural Circuits." *Neuron* 89 (2): 269–284. https://doi.org/10.1016/j.neuron.2015.12.012.

Yang, Y., B. Yao, M. Lei, D. Dan, R. Li, M. van Horn, X. Chen, Y. Li, and T. Ye. 2016. "Two-Photon Laser Scanning Stereomicroscopy for Fast Volumetric Imaging." *PLoS One* 11: e0168885.

VITA